ELSEVIER

Contents lists available at ScienceDirect

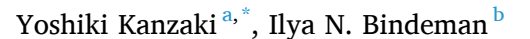
Chemical Geology

journal homepage: www.elsevier.com/locate/chemgeo

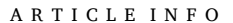


Invited research article

A possibility of ¹⁸O-depleted oceans in the Precambrian inferred from triple oxygen isotope of shales and oceanic crust



- ^a School of Earth and Atmospheric Sciences, Georgia Institute of Technology, Atlanta, GA 30332, USA
- ^b Department of Earth Sciences, University of Oregon, Eugene, OR 97403, USA



Keywords:
Triple oxygen isotope
Weathering
Hydrothermal alteration of oceanic crust
Paleoclimate
Precambrian

ABSTRACT

Oxygen-18/16 ratio recorded in geological media has been utilized to reconstruct surface temperature and discuss associated climatological forcing through Earth's history. The accuracy of the estimated paleotemperature through the application of the δ^{18} O record, however, is limited by our understanding of the oceanic ¹⁸O/¹⁶O ratio in the past. As a longstanding issue, sedimentary rocks in the Precambrian, which are generally depleted in ¹⁸O relative to the modern sediments, can be interpreted either to have reflected higher surface temperature when assuming relatively constant oceanic δ¹⁸O values, or more ¹⁸O-depleted oceans relative to the present day with limited global temperature (climate) deviations. Additional use of a third isotope, ¹⁷O, can help constrain the isotopic composition of the porewater during the formation of a rock record as it provides an additional fractionation equation within the same isotopic system. This study utilizes reactivetransport models of triple oxygen isotope (¹⁶O, ¹⁷O, ¹⁸O) for continental weathering and hydrothermal alteration of oceanic crust, built upon the $\delta^{18}O$ modeling framework developed by Kanzaki (2020a, b). Comprehensive oxygen isotope exchanges in dynamically moving media, both rocks and porewaters, are realized in these models, reflecting spatially-variable and process-dependent alteration conditions (e.g., spreading rate of midocean ridges, uplift rate of continents, porewater advection rate, and isotope exchange kinetics). The models were confirmed to be able to reproduce the signatures of triple oxygen isotope in Phanerozoic shales and oceanic crust. The validated models were then applied to Precambrian shales, which suggests that the Precambrian oceans could have been depleted in 18 O, e.g., as low as -12% at >2.5 Ga and -4% around 0.5 Ga, relative to the present-day seawater. General absence of positive and near-zero $\Delta'^{17}O$ signatures in oceanic crust also suggests that the buffering of oceanic 18O through hydrothermal alteration of the oceanic crust could have been weak. The 18 O flux from continental weathering thus could have played a significant role in controlling the 18 O $^{/16}$ O ratio of ancient sea and together with climatic forcing could have enabled a secular transition of oceanic δ^{18} O during the Precambrian.

1. Introduction

Reconstructing the surface environment in ancient Earth is a key to understanding the evolution of life and the planet. The abundance of and/or ratios among specific elements/isotopes in specific minerals and/or rocks can serve as proxies of paleoenvironments. Among them, the ¹⁸O/¹⁶O ratio of authigenic sedimentary rocks is one of the proxies that have been developed earliest (e.g., Urey et al., 1951) and have been most successful so far (e.g., Veizer and Hoefs, 1976; Veizer et al., 1999). When mineral precipitates in equilibrium with seawater, the oxygen isotopes distribute between the mineral and the seawater according to

the isotope fractionation factor, which is measured as the $\delta^{18}O$ difference between the two phases, $\Delta^{18}O(T)\approx\delta^{18}O_{min}-\delta^{18}O_{sw}$, and whose value depends on temperature. The temperature function for $\Delta^{18}O(T)$ has been determined through laboratory experiments, yielding smaller values with increasing temperature in general (Epstein et al., 1953). The laboratory-established $\Delta^{18}O(T)$ can be utilized for paleo-T reconstruction. However, as seawater in the past cannot be directly sampled and thus there is no historical seawater- $\delta^{18}O$ record, the paleo-T estimation is inevitably based on the measured mineral's $\delta^{18}O$ and the assumed seawater $\delta^{18}O$ value. The major uncertainty in the estimated paleo-T of the oceans comes from what is assumed for the ancient seawater $\delta^{18}O$

E-mail address: ykanzaki3@gatech.edu (Y. Kanzaki).

^{*} Corresponding author.

value, and this topic is a subject of wide disagreements (Walker and Lohmann, 1989; Knauth and Lowe, 2003; Knauth, 2005; Kasting et al., 2006).

Since the early development of the δ^{18} O-based paleo-T estimation method, cumulative research has established that sedimentary rocks, e. g., carbonates, cherts, and shales, (and their component minerals) are more depleted in ¹⁸O at older ages, by as much as 10–15‰ in the Precambrian (e.g., Veizer and Hoefs, 1976; Veizer et al., 1999; Shields and Veizer, 2002; Veizer and Prokoph, 2015; Bindeman et al., 2016; Zakharov et al., 2021, and references therein). These trends have been interpreted with two exclusive paleoclimate scenarios. 1) Higher surface temperatures (as high as >60 °C) during the Precambrian with the δ^{18} O value of seawater having been constant at and invariable from the present-day value (0% relative to the Standard Mean Ocean Water -SMOW) throughout the Earth's history (e.g., Muehlenbachs and Clayton, 1976; Holland, 1984; Muehlenbachs, 1998). 2) Alternatively, a secular oceanic δ^{18} O evolution from a very negative (-10 to -15%) to the present-day value (0%) with the climate and T having been stable and similar to those of the modern Earth (e.g., Veizer et al., 1999; Kasting et al., 2006; Jaffrés et al., 2007), and more hospitable to life.

To resolve the dilemma, the reconstruction of Precambrian and even early Paleozoic seawater δ^{18} O is indispensable. Ophiolites (ancient oceanic crust) have been argued to record seawater $\delta^{18}O$ in their $\delta^{18}O$ profiles, which are similar to oceanic crustal δ^{18} O profiles of the modern Earth and thus have been interpreted to indicate that seawater δ^{18} O has not changed throughout the Earth's history (e.g., Holmden and Muehlenbachs, 1993). The ophiolite record has further been argued to support a hypothesis by Muehlenbachs and Clayton (1976) that seawater δ^{18} O cannot change over $\pm 2\%$ from 0% due to a strong buffering through water-rock interactions at midocean ridges (e.g., Gregory and Taylor, 1981; Holland, 1984), a predominant process that controls seawater $\delta^{18}\text{O}$ value via its long-term (10^6–10^8 yr response time) exchange with the mantle. Changing sedimentary records is typically explained by diagenetic/post-diagenetic overprints with low-δ¹⁸O meteoric waters, the effects of which are argued to increase with age (e.g., Ryb and Eiler, 2018; Liljestrand et al., 2020). A strong argument of the proponents of a temporally constant $\delta^{18}O_{sw}$ is based on global box models that prescribe fluxes and their magnitudes and dependence on $\delta^{18}O_{sw}$, most simply capturing high-T water-rock interaction generating low- δ^{18} O rocks and high- δ^{18} O water, and low-T continental and submarine weathering generating high- δ^{18} O products and sending low- δ^{18} O water into the hydrosphere. In these 0-dimensional box models, ¹⁸O fluxes are balanced between the low- and high-T processes especially spreading of oceanic crust (thus plate tectonic activity), and weathering. However, Kasting et al. (2006) pointed out that the proportion of low and high-T alteration at sea bottom, and its temporal change can torque ocean δ^{18} O values. More generally, the balance/imbalance of ¹⁸O fluxes between the high- and low-T alteration processes have been discussed as a key to enabling variation of oceanic δ^{18} O (e.g., Perry et al., 1978; Walker and Lohmann, 1989; Veizer et al., 1999; Jaffrés et al., 2007; Vérard and Veizer, 2019).

Recently, Kanzaki (2020a, b) pointed out that those studies that support the original Muehlenbachs and Clayton's (1976) hypothesis (e. g., Holland, 1984; Muehlenbachs, 1998) assume not only 0-dimensional box models encompassing the entire Earth's crust and the upper mantle neglecting its potential spatial and temporal heterogeneity, but also assume equilibrium isotope exchange for a half-closed system (open only to a water source/sink but not to a rock source/sink). Indeed, implementation of a 2D model, which more realistically simulates hydrothermal alteration of oceanic crust in a fully open system (Kanzaki, 2020a, b) suggests that age-invariant ophiolite record can alternatively indicate the relative insensitivity of oceanic crust to seawater δ^{18} O due to transport and reaction kinetics and correspondingly weak buffering of oceanic 18 O at ancient midocean ridges.

We here attempt to answer the above questions by utilizing a new tool – triple oxygen isotopes. The addition of ¹⁷O into oxygen-isotope

mass balance provides an extra equation (e.g., Pack and Herwartz, 2014) and allows for resolving temperature and water isotopic values if assumptions are made to connect $\delta^{17}O$ and $\delta^{18}O$ in waters (e.g., Bindeman, 2021). For schematic illustration, here we consider an ideal system where all phases are in equilibrium:

$$\delta^{18}O_{\text{nock}} = \delta^{18}O_{\text{water}} + 10^3 \times \ln\alpha^{18/16}(T)$$
 (1)

$$\delta^{17}O_{\text{rock}} = \delta^{17}O_{\text{water}} + 10^3 \times \ln \alpha^{17/16}(T)$$
 (2)

where $\alpha^{18/16}$ and $\alpha^{17/16}$ are equilibrium fractionation factors for $^{18}{\rm O}/^{16}{\rm O}$ and $^{17}{\rm O}/^{16}{\rm O}$ exchanges that are dependent on T. Additionally assuming that $\delta^{17,18}{\rm O}$ of water is related to one another as in meteoric waters,

$$\delta'^{17}O_{\text{water}} = 0.528 \times \delta'^{18}O_{\text{water}} + y$$
 (3)

where $\delta' \equiv 10^3 \ln{(\delta/10^3+1)}$ (‰) and y is an excess of 17-O which varies from -0.01 to +0.05‰ in most meteoric waters (Luz and Barkan, 2010). The recent advance of research on triple oxygen isotope systematics (Pack and Herwartz, 2014; Sharp et al., 2018; Wostbrock and Sharp, 2021; Zakharov et al., 2021) suggests that differences in fractionations of oxygen isotopes between different media are detectably significant (i. e., the relation of $\delta^{17} O_{rock}$ against $\delta^{18} O_{rock}$ can be significantly different from that expected from the water, Eq. 3). In other words, Eqs. (1)–(3) can be regarded as independent and thus can lead to a solution of paleo-water $\delta^{17,18} O$ and T in theory (e.g., Herwartz, 2021; Miller and Pack, 2021).

Despite its notable merit, there still lingers an uncertainty in the application of triple oxygen isotope systematics to geological records (e. g., Liljestrand et al., 2020; Sengupta et al., 2020; Bindeman, 2021) because natural systems are generally open where (i) reactions especially those at low temperature do not always reach equilibrium as a bulk rock (e.g., Bindeman et al., 2019), and (ii) "water" in Eqs. (1) and (2) are not necessarily isotopically equivalent to source water, i.e., meteoric- or sea-water, depending on the rates of isotope exchanges and water exchange relative to solid-rock transport rate. To reduce the uncertainty, this study utilizes numerical reactive-transport models of triple oxygen isotope representing 1D continental weathering and 2D hydrothermal alteration of oceanic crust. The validity of the models is first confirmed by application to the Phanerozoic and comparison of the computed and observed isotopic compositions of seawater, shales, and oceanic crust. Then, the validated models are applied to the triple oxygen isotope of Precambrian shales and oceanic crust to quantify the δ^{18} O value of seawater during the Earth's earliest eons. Through this exercise, we discuss the $\delta^{18}O_{sw}$ controls by the mode, intensity, and style of plate tectonics (thus of alteration of rocks in the hydrosphere) and highlight insights shed by triple oxygen isotope systematics.

2. Method

2.1. Numerical tools

A reactive transport framework is useful to interpret stable isotopes in natural systems especially where isotope exchanges occur between dynamically moving media. Recently developed reactive-transport models of $^{18}{\rm O}$ and $^{16}{\rm O}$ coupled with an ocean box model by Kanzaki (2020a) reproduce shale and oceanic crustal $\delta^{18}{\rm O}$ data throughout the Phanerozoic. In these models, the computed value of $\delta^{18}{\rm O}_{sw}$ by the ocean box model is shared with the 1D continental weathering and 2D hydrothermal alteration models as a boundary condition, and then the 1D and 2D models return mechanistically simulated $\delta^{18}{\rm O}$ values for rocks and porewaters as well as the corresponding $^{18}{\rm O}$ fluxes that are fed back to the ocean box, leading to consistent $\delta^{18}{\rm O}$ evolutions of the ocean, rocks, and porewaters. We have updated these models to include isotope exchange reactions involving $^{17}{\rm O}$ isotope to simulate triple

oxygen isotope evolution of the oceans, porewaters, and rocks during the Phanerozoic (see below and the Supplement for more details). Furthermore, we have implemented the ¹⁷O isotope and the associated exchange reactions in another 2D model that fully couples hydrothermal fluid circulation and reactive-transport simulations (used in Kanzaki, 2020b and referred to as the "full" 2D hydrothermal alteration model hereafter), to which the simplified 2D hydrothermal model of Kanzaki (2020a) is compared (below and the Supplement). A simple zero-dimensional model for crust alteration (Kanzaki, 2020a) was also updated to enable ¹⁷O-associated reactions, which is useful to illustrate general behaviors of oxygen isotopes in wide parameter space (below and the Supplement).

The governing equations of the updated versions of the above models (0D crust alteration, 1D continental weathering, 2D hydrothermal alteration, 1-box ocean, and full 2D hydrothermal alteration models) can be generalized as (see the Supplement for the details):

$$\frac{\partial^{l} c_{r}}{\partial t} = \nabla \cdot \left(-\mathbf{w}^{l} c_{r} \right) - R^{I/16} - R^{I/II} \tag{4}$$

$$\frac{\partial^{I} c_{p}}{\partial t} = \nabla \cdot \left(-\mathbf{q}^{I} c_{p} + {}^{I} D \nabla^{I} c_{p} \right) + R^{I/16} + R^{I/II}$$
(5)

Here $^{I,II}c_{p,r}$ is the concentration of oxygen isotope $^{I,II}O$ in porewater (with subscript "p") or solid rock ("r"), per unit bulk rock mass (mol kg $^{-1}$) where I and II are 17 or 18; t is time (yr); $R^{I/II}$ is the rate of exchange between ^{I}O in solid rock and ^{II}O in porewater (mol kg $^{-1}$ yr $^{-1}$); $^{I,II}D$ is the coefficient for molecular diffusion plus hydrodynamic dispersion of $^{I,II}O$ in porewater (m 2 yr $^{-1}$); and \mathbf{w} and \mathbf{q} are advection vectors (m yr $^{-1}$) for solid rock and porewater, respectively. The isotope exchange rates are formulated in accord with Cole et al. (1983) as in the original models:

$$R^{I/II} = k^{I/II} \left({}^{I}c_{r}{}^{II}c_{p} - \alpha^{I/II} \times {}^{II}c_{r}{}^{I}c_{p} \right)$$
 (6)

Here, $k^{I/II}$ is the rate constant (mol⁻¹ kg yr⁻¹) where I and II are 16, 17 or 18, with the $k^{18/16}$ value given by the Arrhenius equation in Kanzaki (2020a, b), and kinetic isotope effects are assumed to be negligible (i.e., $k^{18/16} \cong k^{17/16} \cong k^{17/18}$; cf., DePaolo, 2011). The equilibrium exchange fractionation factors for $^{18}\text{O}/^{16}\text{O}$ are formulated as in Kanzaki (2020a, b) and those for $^{17}\text{O}/^{16}\text{O}$ are obtained based on the log-linear relationship between the fractionation factors for $^{18}\text{O}/^{16}\text{O}$ and $^{17}\text{O}/^{16}\text{O}$ exchanges:

$$ln\alpha^{17/16} = \theta ln\alpha^{18/16} \tag{7}$$

where θ is the coefficient for the log-linear relationship. We adopt a temperature function for θ derived by Bindeman et al. (2019):

$$\theta = -\frac{2.05}{T} + 0.5305 \tag{8}$$

Eq. (8) can explain triple oxygen isotope data for modern riverine clays (Bindeman et al., 2019) and is functionally close to the triple oxygen isotope equation for the O-exchange between quartz and water (Sharp et al., 2016) with *T*-dependence being a slightly stronger but not unreasonably so for rock-component minerals (see also Schauble and Young, 2021). Once $\alpha^{17/16}$ is obtained with $\alpha^{18/16}$ and Eqs. (7) and (8), $\alpha^{17/18}$ is calculated as $\alpha^{17/16}/\alpha^{18/16}$. Precambrian meteoric- and seawater $^{17}\text{O}/^{16}\text{O}$ ratios are assumed to change with $^{18}\text{O}/^{16}\text{O}$ ratios following Luz and Barkan (2010) (cf., Eq. 3, see also Herwartz et al., 2015), while rainwater $\delta^{18}\text{O}$ changes with seawater $\delta^{18}\text{O}$ and temperature as in Bowen (2008) (see also Bindeman et al., 2019). This enables us to benchmark our updated models to the previous results (Section 3). See the Supplement for more details on the model modification.

Simulated triple oxygen isotope signatures of rocks and waters are compared with corresponding observations, in which the effects of diagenetic/post-diagenetic overprints are assumed to be minor. Both simulated and observed triple oxygen isotope systematics are presented

with $\delta^{18}O$ and $\Delta'^{17}O_{0.5305}$ relative to SMOW. Here, $\Delta'^{17}O$ is defined as the $^{17}O/^{16}O$ deviation from the mass-dependent fractionation theoretically expected at high temperature, i.e., $\Delta'^{17}O = \delta'^{17}O - 0.5305 \times \delta'^{18}O$, where linearized primed coordinates: $\delta'^{18}O = 10^3 \ln{(\delta^{18}O/10^3 + 1)}$ and $\delta'^{17}O = 10^3 \ln{(\delta^{17}O/10^3 + 1)}$ are used (e.g., Miller et al., 2020). Mantle values for $\delta^{18}O$ and $\Delta'^{17}O_{0.5305}$ are assumed to be 5.7 and - 0.055%, respectively (e.g., Holmden and Muehlenbachs, 1993; Miller et al., 2020). Note that the uncertainty in mantle $\Delta'^{17}O_{0.5305}$ (±0.015%, e.g., Sharp and Wostbrock, 2021) does not significantly affect the results and discussion in this study (Supplement). See Tables 1 and 2 where the major input variables and assumed boundary conditions are respectively tabulated for the 1D and 2D models (see also Section 2.2).

2.2. Boundary conditions during the Precambrian

This section describes assumptions made for the Precambrian simulations because the boundary conditions for the O-isotope models during the Precambrian are less known compared to those during the Phanerozoic (Kanzaki, 2020a; Table 2 and Section 3.2).

2.2.1. Continental weathering model

Surface temperature, uplift/erosion rate, runoff, atmospheric CO_2 level and oceanic $\delta^{18}O$ affect the 1D continental weathering model (Table 1; Kanzaki, 2020a and references therein). Among them, temperature, uplift/erosion rate, and seawater $\delta^{18}O$ are regarded as independent parameters (Section 3.3 and Table 2). The runoff and atmospheric CO_2 levels are both changed as functions of surface temperature, the former based on the temperature dependences of global

 Table 1

 Major input parameters for reactive transport models.

| Isotope | Model | | | | |
|-------------------|--|---|---|--|--|
| signal | 1D continental weathering | 2D hydrothermal alteration | Full 2D hydrothermal alteration | | |
| δ ¹⁸ Ο | Surface temperature (B) | Temperatures of basalt (B), dike (200 °C) and gabbro (350 °C) sections | Seafloor temperature (B) | | |
| | Uplift rate ^c (B) | Water exchanges between basalt, dike and gabbro sections with ocean (B) | Spreading rate (B) | | |
| | Water flux to weathering profile ^c (B) | Thicknesses of basalt (0.5 km), dike (1.5 km) and gabbro (4 km) sections | Pressure at seafloor (25 MPa) | | |
| | Atmospheric CO ₂ concentration (B) | Ridge length (10 ⁵ km) | Ridge length (10 ⁵ km) | | |
| | Weathering enhancement factor ^c (B) | Spreading rate (B) | Depth of mantle- crust interface (6 km) | | |
| | Continental area of igneous and/or high-grade metamorphic rocks (B) | Reactive area (3 \times 10 ⁶ km ²) | Seawater δ ¹⁸ O (B) | | |
| | Rainwater δ^{18} O (B) Unaltered crust δ^{18} O (5.7‰) | Seawater δ^{18} O (B) Unaltered crust δ^{18} O (5.7%) | Unaltered crust $\delta^{18}O$ (5.7‰) | | |
| $\Delta'^{17}O$ | As for δ^{18} O simulation except replacing δ^{18} O with Δ'^{17} O | | | | |

^a Zero-dimensional model is excluded here. See the caption of Fig. 1 for its parameterization adopted in this study.

^b Parameters whose values change with boundary conditions are denoted with "(B)", while those whose values are fixed in this study are denoted with their values in parentheses. For the fixed parameters, the same values as those of the standard or present-day values in Kanzaki (2020a, b) are adopted except for the unaltered crustal $\Delta^{117}O$ (-0.055%).

^c Water flux to weathering profile, weathering enhancement factor and reciprocal of uplift rate are linearly related to the depth of weathering profile (Kanzaki, 2020a; Eq. S28 in Supplement).

Table 2Major boundary conditions assumed for reactive transport models. a,b

| Study ^c | Isotope signal | Age | Model | | |
|--------------------|-----------------------------------|------------------------------|--|----------------------------|---|
| | | | 1D continental weathering | 2D hydrothermal alteration | Full 2D hydrothermal alteration |
| Kanzaki (2020a) | δ ¹⁸ O | Phanerozoic | GEOCARBSULF ^d | GEOCARBSULF ^e | Not used |
| Kanzaki (2020b) | δ^{18} O | Phanerozoic & Precambrian | Not used | Not used | $1/3$ to 10 times present-day spreading rate (3 cm yr $^{-1}$) Present-day seafloor temperature (2 $^{\circ}$ C) |
| This study | $\delta^{18}O \& \Delta'^{17}O f$ | Phanerozoic | GEOCARBSULF ^d | GEOCARBSULF ^e | Present-day spreading rate Present-day seafloor temperature |
| | | Precambrian | CO ₂ greenhouse effect and runoff-temperature relationship according to Kanzaki and Murakami (2018a, b)§ 0.1 to 10 times present-day uplift rate (5 cm kyr ⁻¹) 0 to 60 °C surface temperature 0.135 × or 1.35 × 10^{14} m² of igneous and/or high-grade metamorphic rocks | Not used | 1/3 to 10 times present-day spreading rate Seafloor temperature as a function of surface temperature according to Krissansen-Totton and Catling (2017) |

- ^a Zero-dimensional model is excluded here. See the caption of Fig. 1 for its parameterization adopted in this study.
- $^{\mathrm{b}}$ See Table 1 for parameters whose values change with boundary conditions in this study.
- ^c Assumptions made in the previous studies (Kanzaki, 2020a, b) are listed for comparison.
- d Atmospheric CO₂ concentration, global river runoff, continental area, uplift rate and surface temperature assumed in the GEOCARBSULF model (e.g., Berner, 2006; Royer et al., 2014) are reflected in the relevant parameters (atmospheric CO₂ concentration, water flux to weathering profile, continental area of igneous and/or high-grade metamorphic rocks, uplift rate and surface temperature) in Table 1. Weathering enhancement factor in Table 1 is formulated as a function of atmospheric CO₂ and age as in the GEOCARBSULF model. Rainwater δ^{18} O values are calculated as a function of seawater δ^{18} O and temperature, utilizing functions reported by Dansgaard (1964) and Bowen (2008) (cf. Section 2.1).
- ^e Spreading rate of oceanic crust and surface temperature assumed in the GEOCARBSULF model are reflected in the relevant parameters (spreading rate and temperature of the basalt section) in Table 1. The temperature of basalt section is changed with the surface temperature according to Brady and Gíslason (1997). Water exchanges are linearly related to the spreading rate according to Baker et al. (1996).
- $^{\rm f}$ Δ'¹⁷O values of seawater/rainwater are calculated as a function of δ^{18} O according to Luz and Barkan (2010) and δ^{18} O deviation of rainwater from seawater is calculated as a function of temperature and seawater δ^{18} O according to Bowen (2008) for the Precambrian (Section 2.1).
- ⁸ Atmospheric CO₂ concentration is calculated as a function of luminosity and surface temperature using the temperature-CO₂ relationship by Kanzaki and Murakami (2018b), with reference CO₂ concentrations at given luminosity and surface temperature from von Paris et al. (2008) (see Supplement for the details; Eqs. S25 and S26). Water flux to weathering profile (Table 1) is assumed to linearly change with the global river runoff parameterized as a function of surface temperature by Kanzaki and Murakami (2018a) (Eq. S27 in Supplement). Weathering enhancement factor is parameterized as a square root function of atmospheric CO₂ concentration as in the abiotic mode of the GEOCARBSULF model (Eq. S28 in Supplement).

runoff parameterized by Kanzaki and Murakami (2018a) based on Berner et al. (1983) and Le Hir et al. (2009), and the latter according to the greenhouse effect of atmospheric CO₂ as parameterized by Kanzaki and Murakami (2018b) based on climate models (see Table 2 and Supplement for the details). To include the temperature variations caused by luminosity changes with Earth's age (e.g., Gough, 1981; von Paris et al., 2008) aside from those associated with CO₂ change, four specific ages (0.5, 1.5, 2.5, and 3.8 Ga) are considered (Table 2 and Supplement). As the uplift/erosion rate cannot be determined for the Precambrian, we regard the modern value as the standard value and consider additional two cases where the uplift/erosion is enhanced/weakened by a factor of 10 (Table 2; cf. Husson and Peters, 2017).

For the calculation of 18 O flux via continental weathering during the Precambrian (Section 4), the same assumptions as above are made except for an additional parameter of a continental area composed of igneous and/or high-grade metamorphic rocks (Tables 1 and 2). These rocks react with the hydrosphere and generate a high- δ^{18} O silicate product (sedimentary rocks) while sending low- δ^{18} O flux into the ocean. This weathering flux is primarily torqued by the exposure of these rocks and not sedimentary rocks that are already largely in δ^{18} O equilibrium with the hydrosphere. We consider 2 cases for the continental area available as igneous and/or high-grade metamorphic rocks during the Precambrian: the total land area of the modern Earth (1.35 \times 10¹⁴ m², Amiotte Suchet et al., 2003), and 10% of this area, which has relevance for the Precambrian when less crust emerged and thus was available for weathering (Table 2).

2.2.2. Hydrothermal alteration model

We adopt the full 2D hydrothermal alteration model for the application to the Precambrian in order to reduce the uncertainties (Tables 1

and 2, and Sections 3.3 and 4; Kanzaki, 2020b). Changes in the spreading rate of oceanic crust (e.g., Muehlenbachs and Clayton, 1976; Holland, 1984) and the seafloor temperature are dominant parameters to affect the calculation of ¹⁸O flux via hydrothermal alteration (Table 1; Kanzaki, 2020a, b). The spreading rate is assumed to be either the same as the present-day value or modified by a factor of 1/3, 3, or 10, similar to the one considered by Kanzaki (2020b) for the Precambrian hydrothermal conditions. Seafloor temperature is changed with the surface temperature following Krissansen-Totton and Catling (2017) (Table 2).

3. Results

3.1. General isotope behavior as a function of fundamental alteration variables

Stable isotope geochemists (Taylor, 1968) long implicitly assumed that water-rock interaction may not necessarily be complete, and thus, waters may get variably "shifted" isotopically, depending on the exchange kinetics in modern meteoric hydrothermal systems, or on static rocks (i.e., half-closed systems). However, the currently predominant box model of global fluxes on O isotope exchange (e.g., Holland, 1984; Muehlenbachs, 1998) assumes strong rock-water coupling, which we challenge in this work. Fig. 1 shows the effects of the water/rock ratio (ψ) and the degree of oxygen isotope exchange (κ) on the coupling between the seawater and rocks. The two parameters, ψ and κ , quantify the above isotopic shifts in a fully open system (i.e., on moving rocks) and are defined as the rates of porewater-ocean exchange and oxygen isotope exchanges relative to the solid-rock transport rate, respectively (i.e., $\psi \propto |\mathbf{q}|/|\mathbf{w}|$ and $\kappa \propto k^{I/II}/|\mathbf{w}|$; see the Supplement for more details). Therefore, the behavior of O isotopes in a natural system can be

Y. Kanzaki and I.N. Bindeman Chemical Geology 604 (2022) 120944

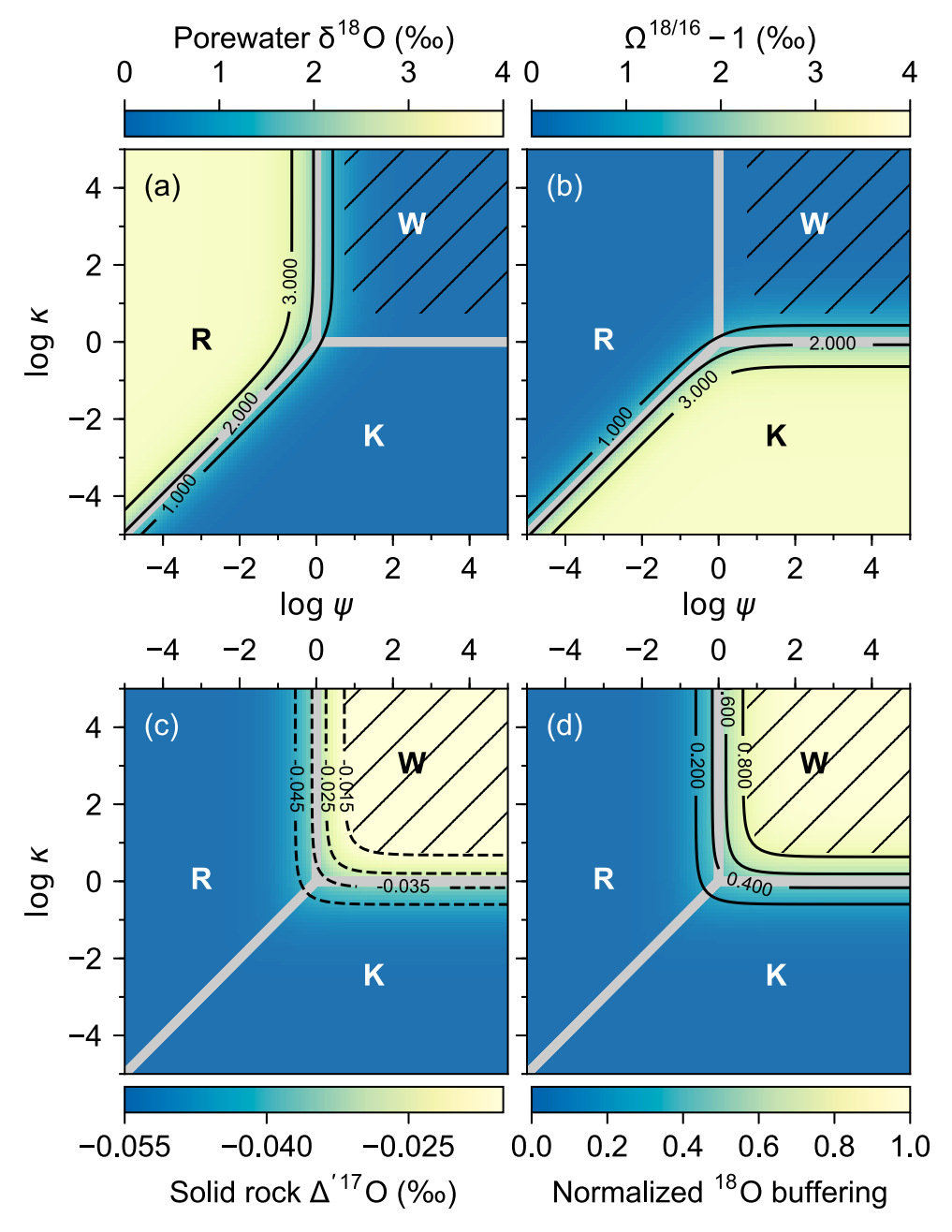


Fig. 1. Relationship between parameters ψ (relative rate of seawater-porewater exchange against solid-rock supply/sink) and κ (relative rate of isotope exchange). Panels show: (a) porewater δ^{18} O, (b) distance from isotope exchange equilibrium, (c) solid-rock $\Delta'^{17}O$ and (d) seawater- $\delta^{18}O$ buffering intensity, during hydrothermal alteration of oceanic crust. Typical parameter values for high-temperature hydrothermal alteration are adopted $(10^3 ln\alpha_{rock-water}^{18/16} = 2, 6 \times 10^5$ $\,\text{km}^2$ depth $\,\times\,$ width of crust with 0.1 porosity, 3 cm yr^{-1} spreading rate, 3×10^3 and 1×10^3 kg m⁻³ of crust particle and water density, respectively, and 31.3 and 55.6 mol kg^{-1} of oxygen for solid rock and porewater, respectively) as assumed in Kanzaki (2020a) except with an additional coefficient for the log-linear relationship between ¹⁸O/¹⁶O and ¹⁷O/¹⁶O fractionation factors, which has been taken to be 0.527 (e. g., Sharp et al., 2016). Note that in (d) the buffering intensity is normalized by the strong buffering intensity proposed by Holland (1984). Shaded areas represent the ψ-κ parameter space that is inconsistent with oceanic crustal (<-0.015%).

described by a combination of the parameters ψ and κ . As an example, Eqs. (1)–(3) can be applicable to geological records only if one can assume fast kinetics for both O-exchange reactions and overwhelming water transport ($\kappa \gg 1$ and $\psi \gg 1$).

Generally, it is shown that the oxygen isotope behavior during crust alteration can be classified into 3 cases depending on ψ and κ (Fig. 1): (i) the water-buffered equilibrium case as $\psi \to \infty$ and $\kappa \to \infty$ ("W" in Fig. 1; Eqs. 1–3), (ii) the rock-buffered equilibrium case as $\psi \to 0$ with any $\kappa \gg \psi$ ("R" in Fig. 1), and (iii) the reaction-limited case as $\kappa \to 0$ with any $\psi \gg \kappa$ ("K" in Fig. 1). Note that the coupling of oxygen isotopes between altered oceanic crust and seawater and the buffering intensity of oxygen isotopes in seawater by alteration of the oceanic crust can become as strong as previously assumed in box-models (e.g., Holland, 1984; Muehlenbachs, 1998), only in case (i) ("W" in Fig. 1). However, Kanzaki (2020a) pointed out that case (i) is not accomplished under most hydrothermal alteration conditions. In particular, the heat budget of the Earth could be violated if case (i) dominates the Earth's hydrothermal

alteration condition because it would deplete the heat of oceanic crust by hydrothermal fluids, which is not observed.

As a merit of adding 17 O to the mass balance of O isotopes in hydrothermal alteration, one may be able to extract additional information on alteration conditions. Indeed, the observed range of oceanic crustal Δ'^{17} O values (generally <-0.015%; Sharp et al., 2018) is expected only when case (i) is largely excluded (shaded areas in Fig. 1).

3.2. Model validation: Phanerozoic oceans, oceanic crust and shales

The modified models of this study reproduce Phanerozoic crustal and shale $\delta^{18}O$ data as well as the original models (Figs. 2 and 3). Additional results for $\Delta'^{17}O$ are also comparable to the modern and Phanerozoic $\Delta'^{17}O$ observations (Figs. 2 and 3). Specifically, the computed $\Delta'^{17}O$ for altered continental and oceanic rocks show the same trend as observed in Phanerozoic shales and oceanic crust (Figs. 2d and 3a), and at the same time, the present-day seawater $\Delta'^{17}O$ is consistent between the

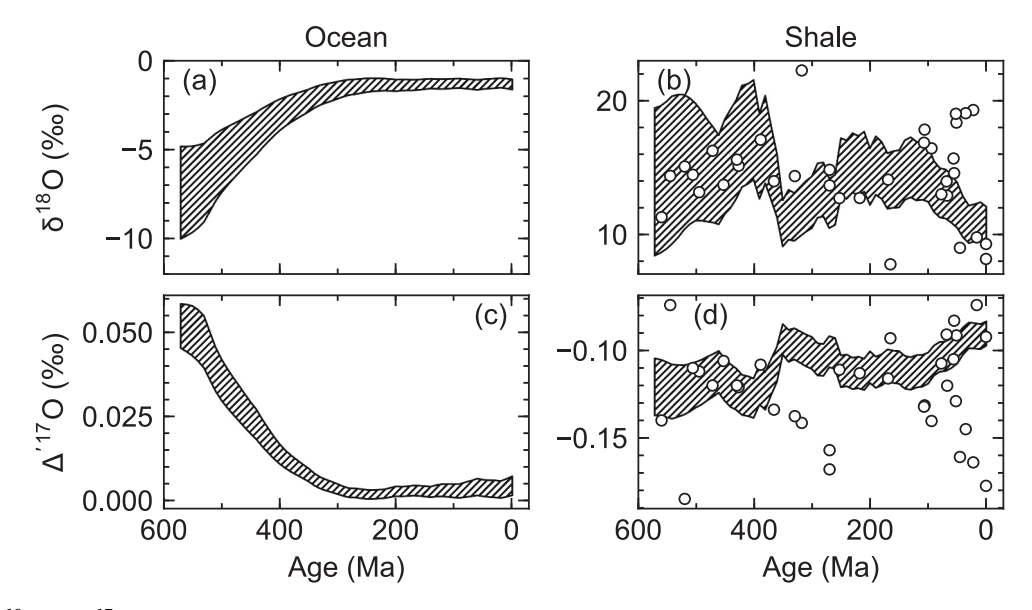


Fig. 2. Evolution of $\delta^{18}O$ and $\Delta'^{17}O$ of Phanerozoic seawater (a, c) and shales (b, d) simulated by the modified models of ocean box, 1D continental weathering, and 2D hydrothermal alteration of oceanic crust. Measured $\delta^{18}O$ and $\Delta'^{17}O_{0.5305}$ values for Phanerozoic shales are from Bindeman et al. (2018) and Bindeman (2021).

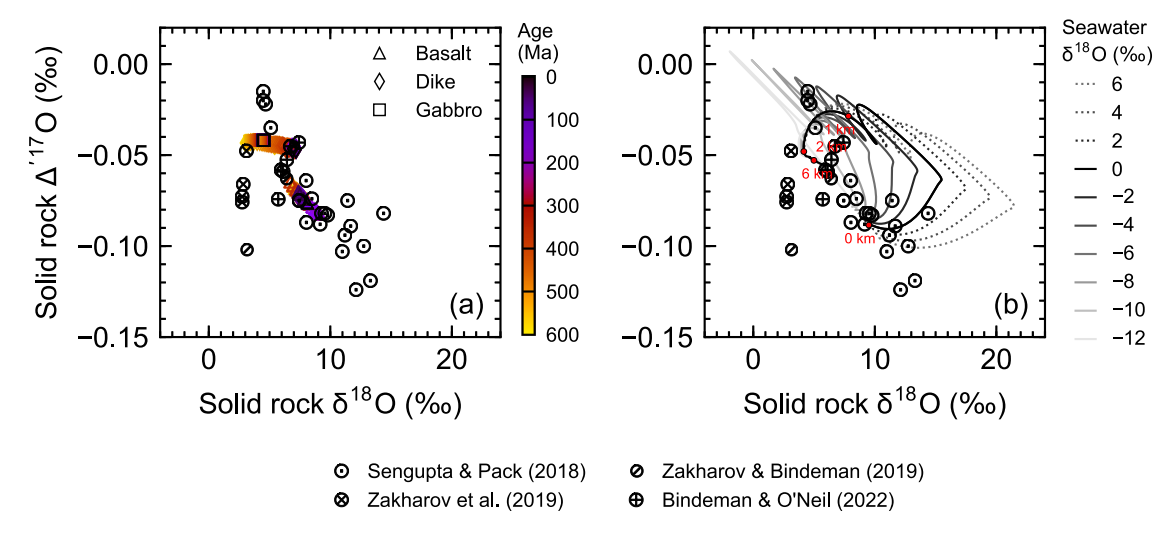


Fig. 3. Triple oxygen isotope of hydrothermally altered oceanic crust simulated by the modified 2D hydrothermal alteration models as compared to observations. (a) Evolution trends for pillow basalt, sheeted dike and gabbro sections as a function of age during the Phanerozoic, modeled by the simple 2D model (using seawater O-isotopic composition in Figs. 2a, c). (b) Implementation of the full 2D hydrothermal alteration model as a function of seawater δ^{18} O. In b, depths of oceanic crust at 0, 1, 2 and 6 km are denoted by red circles with corresponding annotations only in the case with 0‰ of seawater δ^{18} O (black solid curve). The calculated isotopic composition moves clockwise from the mantle values at greater depths, reflecting slower kinetics of water-rock interaction, increasing fractionation factors, and increasing water/rock ratios at shallower depths with lower temperatures. Notice that most of data points can be explained by the model with any of the assumed δ^{18} O_{Sw} values (–12 to 6‰). (For interpretation of the references to colour in this figure legend, the reader is referred to the web version of this article.)

calculation and observation (0‰ at 0 Ma, Fig. 2c). The results for oceanic crustal $\Delta'^{17}{\rm O}$ plotted against $\delta^{18}{\rm O}$ by the 2D hydrothermal alteration model (Fig. 3a) are also consistent with those by the full 2D model (Fig. 3b). This confirms that the simplified parameterization by Kanzaki (2020a) can capture the general features of triple oxygen isotope in hydrothermal systems. Note, however, that the diverse $\Delta'^{17}{\rm O}$ values at low $\delta^{18}{\rm O}$ (from -0.100 to -0.015% of $\Delta'^{17}{\rm O}$ at <5% of $\delta^{18}{\rm O}$, Fig. 3) can only be reproduced by the full 2D model as it can better realize the heterogeneity of hydrothermal systems (Supplement; cf. Farahat et al., 2017; Zakharov et al., 2021). Overall, the modified models are capable of reproducing signatures of $\Delta'^{17}{\rm O}$ as well as $\delta^{18}{\rm O}$ in the Phanerozoic oceans, oceanic crust and shales.

3.3. Application to Precambrian oceanic crust and shales

3.3.1. Oceanic crust

Oceanic crustal ${\Delta'}^{17}O$ data in the Precambrian is similar to those in the Phanerozoic (e.g., Zakharov and Bindeman, 2019; Zakharov et al., 2019; Bindeman and O'Neil, 2022). Because the dataset for preserved and studied sections of oceanic crust of the Precambrian age is limited compared to shales (cf. Section 3.3.2), we assume that triple oxygen isotope signature (e.g., data points in the $\delta^{18}O$ - $\Delta'^{17}O$ space) does not significantly change with age as is the case for $\delta^{18}O$ (e.g., Gregory, 1991). We thus consider the alteration conditions, including seawater $\delta^{18}O$ value, that could explain the overall oceanic crustal data available of any age. As described in Section 3.1, the water-buffered equilibrium case ($\kappa \gg 1$ and $\psi \gg 1$) is unlikely to have been the predominant

subseafloor alteration condition during the Precambrian. More plausible alteration conditions are thus characterized by either the reaction-limited case or by rock-buffered equilibrium case, or the combination of the two, which is consistent with the simple and full 2D hydrothermal alteration models (Figs. 1 and 3). Note, however, that the water-buffered equilibrium condition can develop locally within a limited 2D section, which can be recognized by a relatively high solid-rock $\Delta^{\prime\,17}{\rm O}$ within limited depth intervals (e.g., spikes approaching 0% of $\Delta^{\prime\,17}{\rm O}$ in Fig. 3b; see also the Supplement).

Under such alteration conditions, oceanic crustal rocks are partially decoupled from the seawater with respect to full exchange of oxygen isotopes. Accordingly, a wide range of seawater $\delta^{18}O$ can explain the age-invariant triple oxygen isotope signature of oceanic crust (e.g., Fig. 3b) and seawater δ^{18} O buffering at midocean ridges can be weaker than expected from a water-buffered equilibrium case, e.g., Holland (1984) and Muehlenbachs (1998) (cf. Section 4.1). As an example, with the full 2D model where the hydrothermal circulation changes with the spreading rate, a wide range of seawater δ^{18} O, from -8 to 0%, can explain the oceanic crust and ophiolites with the present-day spreading rate, although the constrained range can change to less than -10% and more than -2%, when the spreading rate is reduced and enhanced, respectively, by a factor of 3 (Kanzaki, 2020b). Therefore, if one order of magnitude uncertainty is allowed for the spreading rate from the present-day value, seawater δ^{18} O cannot be constrained by δ^{18} O of ophiolites and oceanic crustal rocks at all. Accordingly, invariant triple oxygen isotope data from the oceanic crust is difficult to utilize for constraining seawater δ^{18} O unless the alteration conditions including the spreading rate are precisely known as inferred by Kanzaki (2020b) who only considered δ^{18} O. On the other hand, subaerial alteration of continental rocks into weathering products and shales is strongly coupled to the reacting fluids, and thus can be less decoupled from seawater with respect to oxygen isotopes, given well-constrained $\delta^{17,18}O$ relationships between sea- and meteoric-water (Bowen, 2008; Luz and Barkan, 2010; Section 2.2) (see the next section).

3.3.2. Shales

Bindeman et al. (2018) showed the transition of triple oxygen isotope in shales over the Precambrian. The shifts of the Precambrian shales in the $\delta^{18}\text{O-}\Delta'^{17}\text{O}$ space should be able to be reproduced by the 1D continental weathering model when provided with appropriate alteration conditions, as it can reproduce the Phanerozoic shale record (Figs. 2b and d). Due to the uncertainties in the parameters which can affect the 1D continental weathering model, however, a series of simulations are conducted especially focusing on the effects of temperature, uplift/ erosion rate and seawater δ^{18} O variations (Section 2.2, Table 2 and Supplement for the details). Figs. 4-6 show the surface rock triple oxygen isotope signature at three different uplift/erosion rates (the modern (default) and 0.1/10 times weakened/enhanced rates) under various luminosity for four specific Earth's age (0.5, 1.5, 2.5, and 3.8 Ga; 4 panels in each figure). Trajectories depicted as curves therein illustrate the effects of temperature variations including those of runoff and atmospheric CO₂ (Section 2.2; Table 2; Supplement). To facilitate comparison, shale data are divided into four bins according to their ages (0-1, 1-2, 2-3 and 3-4 Ga), and each panel of Figs. 4-6 depicts with bright colors only those from the bin whose age range covers its assumed Earth's age but the rest with pale colors.

When the uplift rate is relatively fast (e.g., Fig. 6) or exchange rates are relatively slow (e.g., at relatively low T in Figs. 4–6), altered continental rocks are not in isotope exchange equilibrium ("K" in Fig. 1). In this reaction-limited regime, increasing temperature (and atmospheric CO_2 and runoff) drives the altered-rock isotope signature from the pristine mantle values to equilibrium values, the trajectory of which is dependent upon seawater $\delta^{18}O$ and the temperature at which the equilibrium is first attained (denoted hereafter as "equilibrium temperature"). When the equilibrium temperature is low (e.g., with the low uplift rate or luminosity, meaning long reaction duration or high atmospheric CO_2 , respectively), θ in Eq. (8) is more deviated and smaller than the high-temperature value of 0.5305 and thus a slope of the trajectory in the $\delta^{18}O$ - $\Delta'^{17}O$ space along increasing temperature becomes

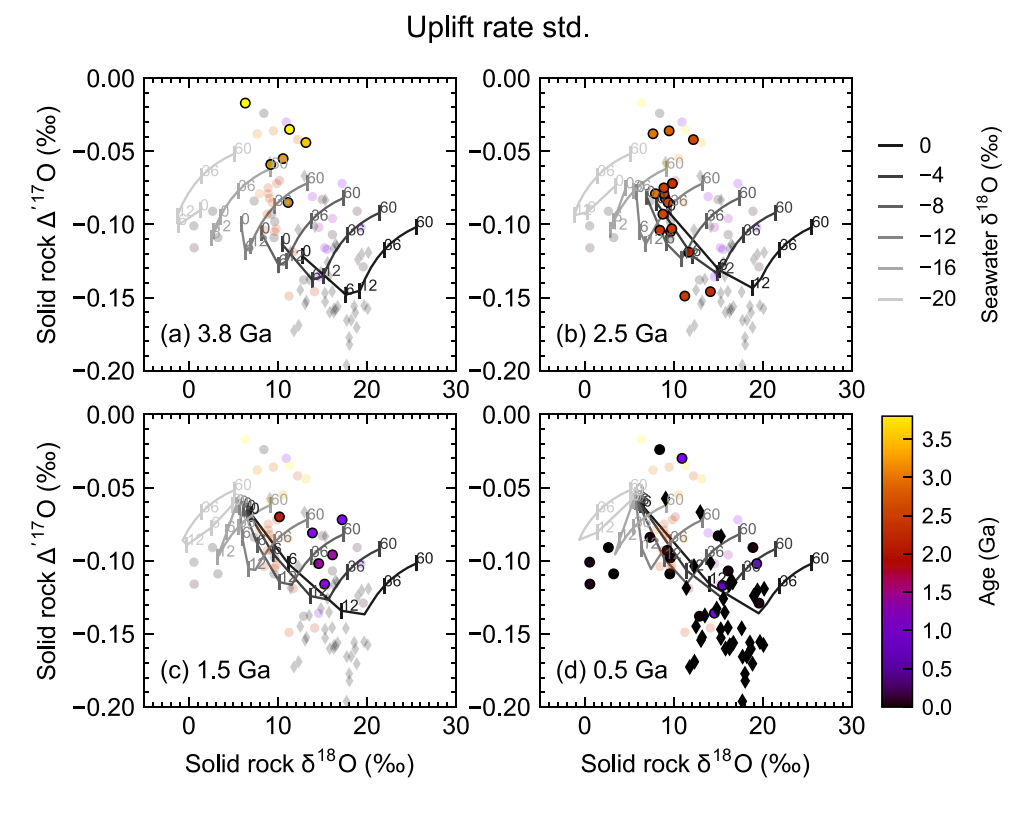


Fig. 4. Triple oxygen isotope of shales simulated by the modified 1D continental weathering model as a function of seawater $\delta^{18} \text{O}$ values and surface temperatures. The model assumes the present-day uplift rate and 0-60 °C range of surface temperature (0, 6, 12, 36, and 60 °C marked). The model was run under solar luminosity at 3.8 (a), 2.5 (b), 1.5 (c) and 0.5 (d) Ga. The model also takes into account atmospheric CO2 and runoff changes along with T change (Section 2.2). Observed shale data (circles) are from Bindeman et al. (2018) and Bindeman (2021). Also shown are the modern river clay data (black diamonds) from Bindeman et al. (2019) for comparison. To facilitate the simulation-observation comparison, shale and modern clay data are divided into four bins depending on ages (0-1, 1-2, 2-3 and 3-4 Ga) and each panel depicts data with bright colors only if they are from the bin whose range of age includes the Earth's age assumed for luminosity else with pale colors. Note that although $\delta^{18}O$ and $\Delta'^{17}O$ values in reacting meteoric waters change with contemporaneous seawater and T (e.g., Bindeman et al., 2019), they are not shown here for simplicity. Further notice that horizontally extending shale data at 0.5 Ga are better explained with a moderately depleted $\delta^{18}O_{sw}$ (e.g., -4%) while more vertically variable data in the Archean by a low δ18Osw (e.g., -12%).

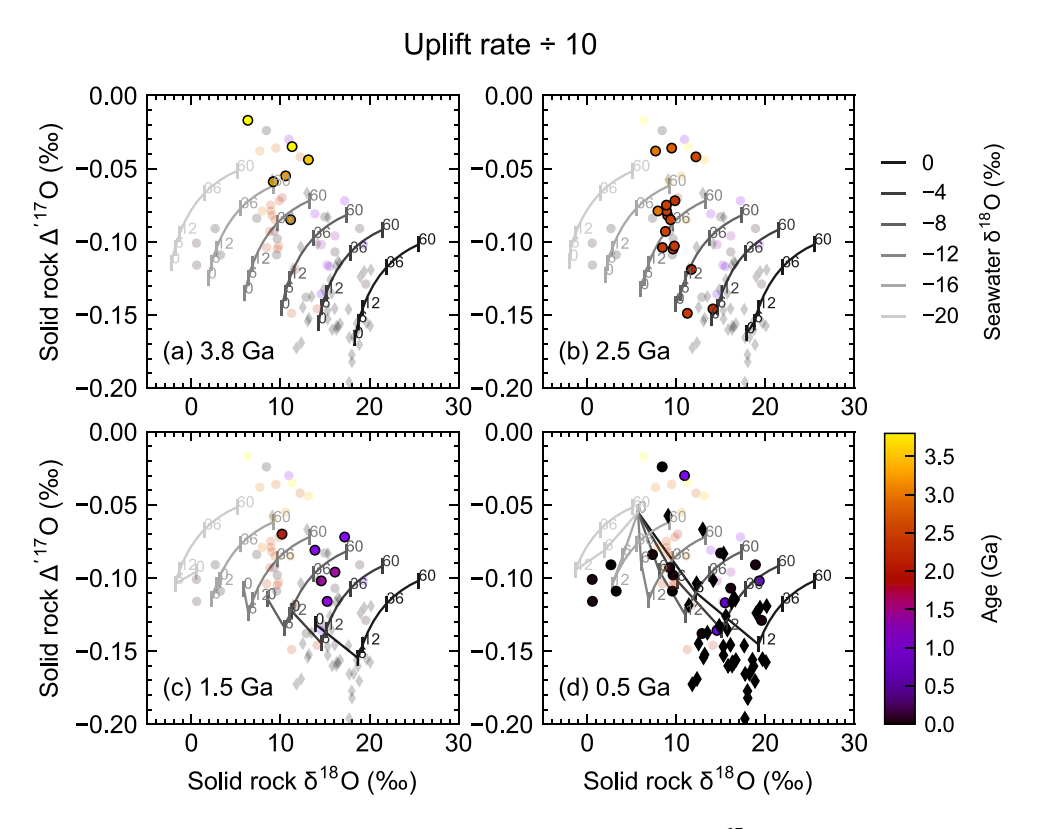


Fig. 5. As for Fig. 4 except with the slower uplift rate (\times 0.1) assumed for the calculation. Notice that $\Delta'^{17}O_{0.5305}$ is more negative and vertically extending $\delta^{18}O_{0.5305}$ trends are more often simulated compared to Fig. 4.

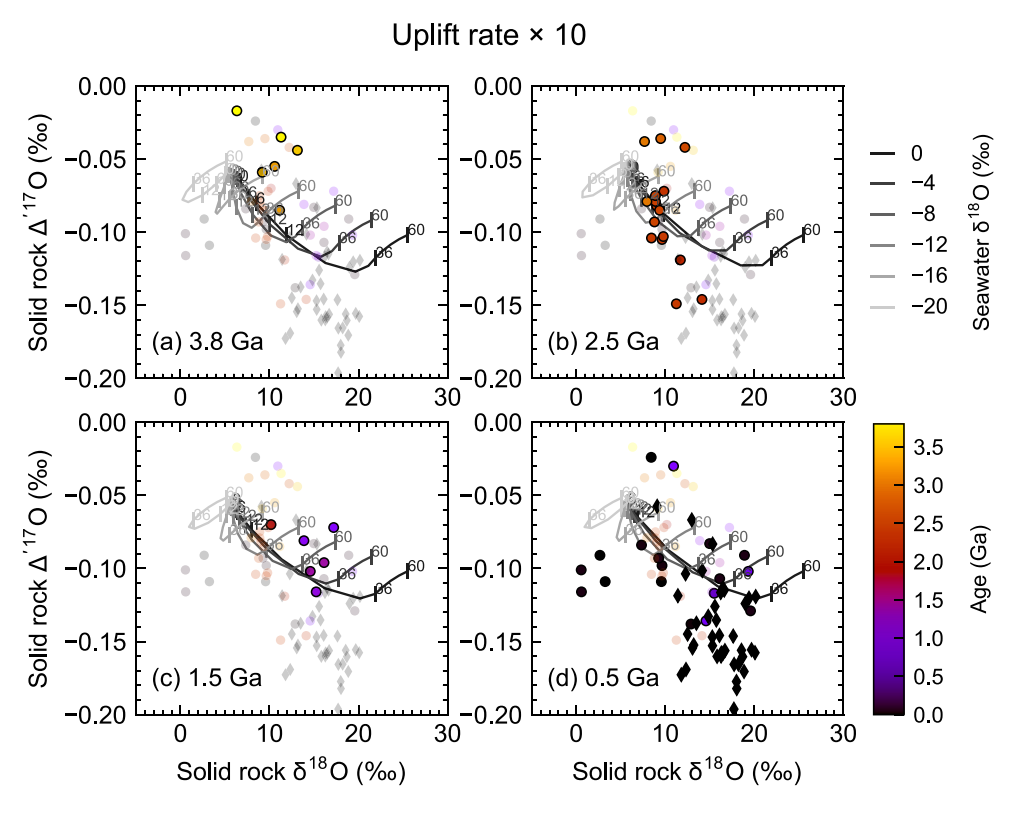


Fig. 6. As for Fig. 4 except with the higher uplift rate (\times 10) assumed for the calculation. Notice that ${\Delta'}^{17}O_{0.5305}$ is less negative and horizontally extending $\delta^{18}O_{0.5305}$ trends are more often simulated compared to Fig. 4.

Y. Kanzaki and I.N. Bindeman Chemical Geology 604 (2022) 120944

steeper for a given seawater δ^{18} O. Also, seawater δ^{18} O determines the equilibrium isotopic signature of altered rock and thus the trajectory to the triple isotope data-point at the equilibrium temperature. As an example, increases in T result in increases of altered-rock $\delta^{18}O$ only when the equilibrium rock δ^{18} O is larger than the mantle value (e.g., seawater $\delta^{18}O>-16\%$). Consequently, when isotope exchanges of bulk rock are reaction-limited (e.g., T < 12-18, 0–12, and 36 °C in Figs. 4–6, respectively), δ^{18} O and Δ'^{17} O values increase and decrease, respectively, from the pristine values as temperature increases, except for the case with a low seawater δ^{18} O (e.g., <-16%) where the rock δ^{18} O decreases with temperature to approach an equilibrium rock $\delta^{18}O$ that is lower than the mantle value. Above the equilibrium temperature, altered rock isotope signature is more affected by changes of $\delta^{18}O$ and $\Delta^{\prime 17}O$ in meteoric waters (not shown) in addition to equilibrium fractionation factors ("W" in Fig. 1), and thus both δ^{18} O and Δ'^{17} O increase with T (Bowen, 2008; Luz and Barkan, 2010).

Shale data shifts from horizontally diverse data in the $\delta^{18}O$ - $\Delta'^{17}O$ space extending to larger δ^{18} O and lower $\Delta^{\prime 17}$ O values during the Phanerozoic to more vertically diverse data characterized with smaller δ^{18} O but allowing larger $\Delta^{\prime 17}$ O. Such a trend change in the δ^{18} O- $\Delta^{\prime 17}$ O space can be interpreted as a shift from the reaction-limited regime with a seawater δ^{18} O that is relatively close to the present-day value (up to -4% at 0.5 Ga) to the equilibrium conditions reflecting triple oxygen isotope signature of meteoric waters formed from more ¹⁸O-depleted seawaters (down to -12% at >2.5 Ga), without necessitating a drastic change in T. The above interpretation of the Precambrian shales is valid regardless of the uplift rate (Figs. 4-6) although, in the high uplift rate case (Fig. 6), shale data for the early Archean could also be explained with the reaction-limited regime with a relatively low T and high seawater $\delta^{18}O$ (e.g., 0-6 °C and 0‰, respectively, in Fig. 6a). This alternative interpretation, however, cannot be supported because the high uplift rate would likely have led to a large ¹⁸O flux from continental weathering and thus a negative steady-state seawater $\delta^{18}O$ (Section 4.1) and also because the combination of the low T and 0% of seawater δ^{18} O contradicts δ^{18} O records of other sedimentary rocks (Section 4.2).

4. Discussion

4.1. Control on oceanic δ^{18} O in the Precambrian

Out of several factors controlling $\delta^{18}O_{sw}$ (e.g., Wallmann, 2001; Jaffrés et al., 2007) high/low-T hydrothermal alteration at midocean ridges and continental weathering constitute >95% of all fluxes (Muehlenbachs, 1998; Holland, 1984). In accord with this, we only

consider continental weathering and oceanic crust alteration as the major ¹⁸O sources/sinks in this section (e.g., Kasting et al., 2006; Kanzaki, 2020a).

Precambrian oceanic crust and shales can be explained by a negative seawater $\delta^{18}O$ and a temperate climate (Section 3). The negative value of seawater $\delta^{18}O$ during the Precambrian needs to be consistent with the fluxes of oxygen isotopes to the oceans from continental and oceanic crust alteration at the same time. There are greater uncertainties in the parameter values necessary to assume for the Precambrian compared to the Phanerozoic. These include area, composition and uplift rate of continents, and spreading rate of oceanic crust (Section 2.2 and Table 2). As such, we consider the potential magnitudes of ^{18}O fluxes from continental weathering and oceanic crust alteration for various combinations of these relevant alteration-parameter values. A plot of these fluxes as a function of seawater $\delta^{18}O$ is useful to consider the relative magnitudes of fluxes from different processes and determine seawater $\delta^{18}O$ at the steady state where the net $\delta^{18}O$ flux is zero (e.g., Muehlenbachs and Clayton, 1976; Muehlenbachs, 1998).

As an illustration of the utility of the 18 O flux vs. seawater δ^{18} O plot (Fig. 7), we first present the results for the Phanerozoic application conducted in Section 3.2. Figs. 7a and b show the ¹⁸O fluxes resulting from continental weathering and oceanic crust alteration, respectively, plotted against seawater δ^{18} O during the Phanerozoic. Slopes in these diagrams represent the oceanic-¹⁸O buffering intensity through either process, with a steeper slope corresponding to a stronger oceanic-¹⁸O buffering. One can recognize that oceanic crust alteration has the stronger control on seawater δ¹⁸O during most of the Phanerozoic except for a period in the Paleozoic (orange lines in Fig. 7) when both alteration processes have comparable contributions. A hypothetical steady-state seawater δ^{18} O for a given process is defined by assuming that this process alone controls the oceanic ¹⁸O budget and thus can be calculated as an intercept at zero ¹⁸O flux for the process (arrows in Figs. 7a and b). Actual steady-state seawater δ^{18} O reflects all the relevant processes, i.e., both continental weathering and oceanic crust alteration. The seawater $\delta^{18}O$ value is determined as an intercept of zero net flux (e.g., arrows in Fig. 7c), and equal to an average of the hypothetical steady-state values for all the relevant processes (e.g., intercepts at zero fluxes in Figs. 7a and b) weighted by the oceanic-¹⁸O buffering intensity (slopes in Figs. 7a and b) (see the Supplement for the details). In the Phanerozoic application, seawater $\delta^{18}O$ deviates from the value buffered at midocean ridges (\sim 0%, Fig. 7b) and gets closer to a negative value buffered by continental weathering (-14 to -13%, Fig. 7a) only during the Paleozoic when the buffering intensity by continental weathering becomes comparable to that by oceanic crust alteration. At

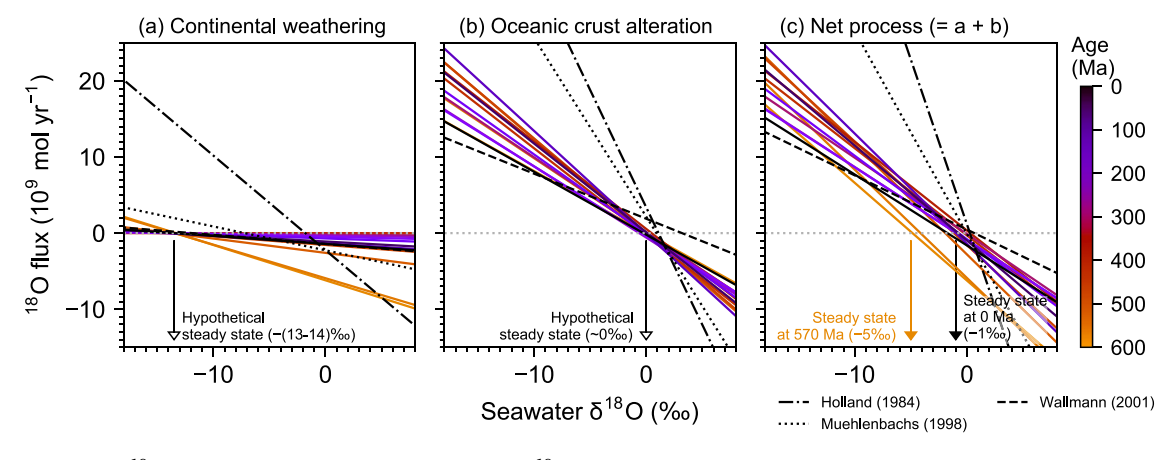


Fig. 7. Effects of seawater $\delta^{18}O$ composition during the Phanerozoic on the ^{18}O fluxes from continental weathering (a) and hydrothermal alteration of oceanic crust (b), and the total ^{18}O flux from both processes (c). Hypothetical steady-state values of seawater $\delta^{18}O$ are determined by assuming that a process governs the ocean ^{18}O budget alone (i.e., arrows in a and b where ^{18}O flux = 0). The actual steady-state value (arrows in c where ^{18}O flux = 0) is the average of hypothetical steady-state values weighted with ^{18}O -buffering intensities (slopes in a and b) for continental and oceanic crust alteration. Fluxes from three prior studies are shown for comparison.

570 Ma, for instance, the contribution of continental weathering is increased to 36%, resulting in -5% of steady-state seawater δ^{18} O, which should be compared with the situation at 0 Ma where the contribution is only 11% with a steady-state ice-free seawater δ^{18} O of -1% (Fig. 7c). The enhanced contribution of continental weathering to the 18 O budget during the Paleozoic has been attributed to higher atmospheric CO₂ and a greater land area of exposed igneous and high-grade metamorphic rocks (Kanzaki, 2020a).

Also shown in Fig. 7 are the results from previous studies by Holland (1984) and Muehlenbachs (1998) that report $^{18}{\rm O}$ fluxes from both weathering and hydrothermal alteration. The estimates were made by these authors assuming that isotope fractionation occurs always linearly proportional to seawater $\delta^{18}{\rm O}$ as is the case for a water-buffered equilibrium system (cf. Eqs. 1, 2). Thus, their estimates tend to overestimate the $^{18}{\rm O}$ buffering intensity, yielding steep slopes in Fig. 7. The estimates by Wallmann (2001) (dashed lines) are relatively close to those by Kanzaki (2020a) and this work (solid lines). The $^{18}{\rm O}$ fluxes in Wallmann's model are all assumed to scale with the spreading rate and thus relative contributions from weathering and hydrothermal alteration do not change with age, resulting in a constant steady-state seawater $\delta^{18}{\rm O}$ throughout the Phanerozoic (Wallmann, 2001; see also Kanzaki, 2020a). Using the reactive transport models for calculation of $^{18}{\rm O}$ fluxes from

rock alterations, as in Kanzaki (2020a) and this work, allows for explicit reflection of changes in alteration conditions in the evolution of steady-state seawater δ^{18} O (solid lines in Fig. 7).

The ¹⁸O fluxes to the Precambrian oceans through crust alteration are significantly affected by the assumed uplift rate and weathering area of igneous/metamorphic areas on continents, and the spreading rate of oceanic crust (Figs. 8 and 9, with the solar luminosity at 3.8 Ga; see below for the effects of the luminosity variation). The ¹⁸O flux and associated hypothetical steady state $\delta^{18}O_{sw}$ values from the seafloor alteration are mostly determined by the spreading rate, and their dependence on the surface temperature is relatively minor (Section 3.3.1; panels b, e and h in Figs. 8 and 9). The surface temperature affects the ¹⁸O flux from the continental weathering because atmospheric CO₂ and the amount of riverine runoff also change with temperature (Section 2.2.1). These together determine $\delta^{18}O$ profiles of subaerially altered rocks (Section 3.3.2), and correspondingly, hypothetical steady state $\delta^{18}O_{sw}$ values (panels a, d and g in Figs. 8 and 9). At a relatively high temperature (e.g., T > 12-18 °C in Fig. 8a), isotope exchange reactions are in the water-buffered equilibrium regime ("W" in Fig. 1) and the ¹⁸O buffering intensity through continental weathering (slopes in panels a, d and g of Figs. 8 and 9) reaches a maximum (cf. Fig. 1d) and does not change further with temperature under given tectonic condition (i.e.,

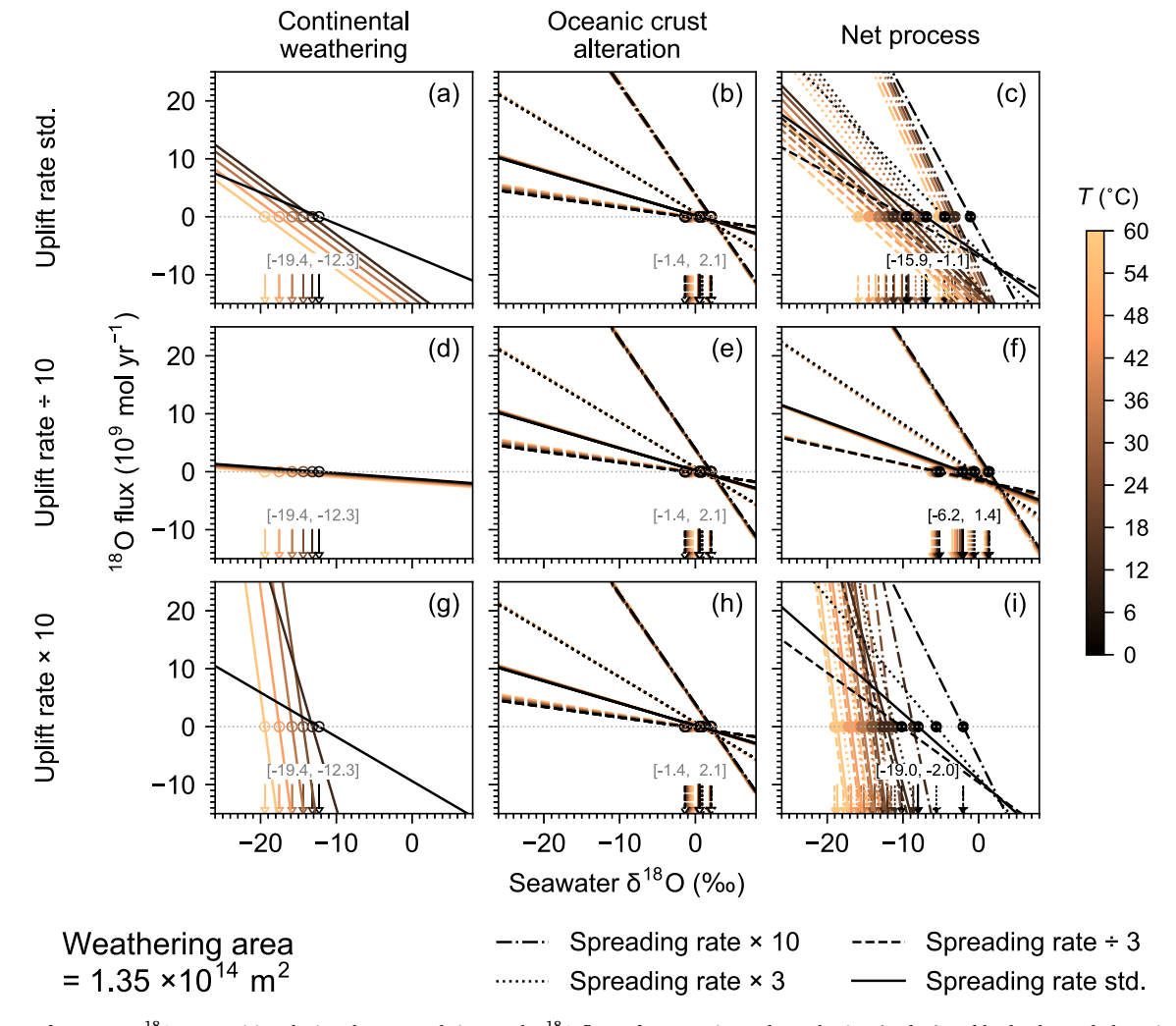


Fig. 8. Effects of seawater $\delta^{18}O$ composition during the Precambrian on the ^{18}O fluxes from continental weathering (a, d, g) and hydrothermal alteration of oceanic crust (b, e, h), and the total ^{18}O flux from both processes (c, f, i). The relevant alteration parameters are assumed as follows: 0 to 60 $^{\circ}C$ for the surface temperature, the present-day value (a, b, c) or a modified value by a factor of 10 (d–i) for the uplift rate, the modern land area for the area of igneous and/or high-grade metamorphic rocks, the present-day value or that multiplied by a factor of 1/3, 3 or 10 for the spreading rate of oceanic crust, and solar luminosity at 3.8 Ga. Arrows show (hypothetical) steady-state $\delta^{18}O_{sw}$ values whose ranges are denoted in square brackets. Notice that a negative $\delta^{18}O_{sw}$ resulted unless the uplift rate was smaller than the present day by a factor of 10 (d–f).

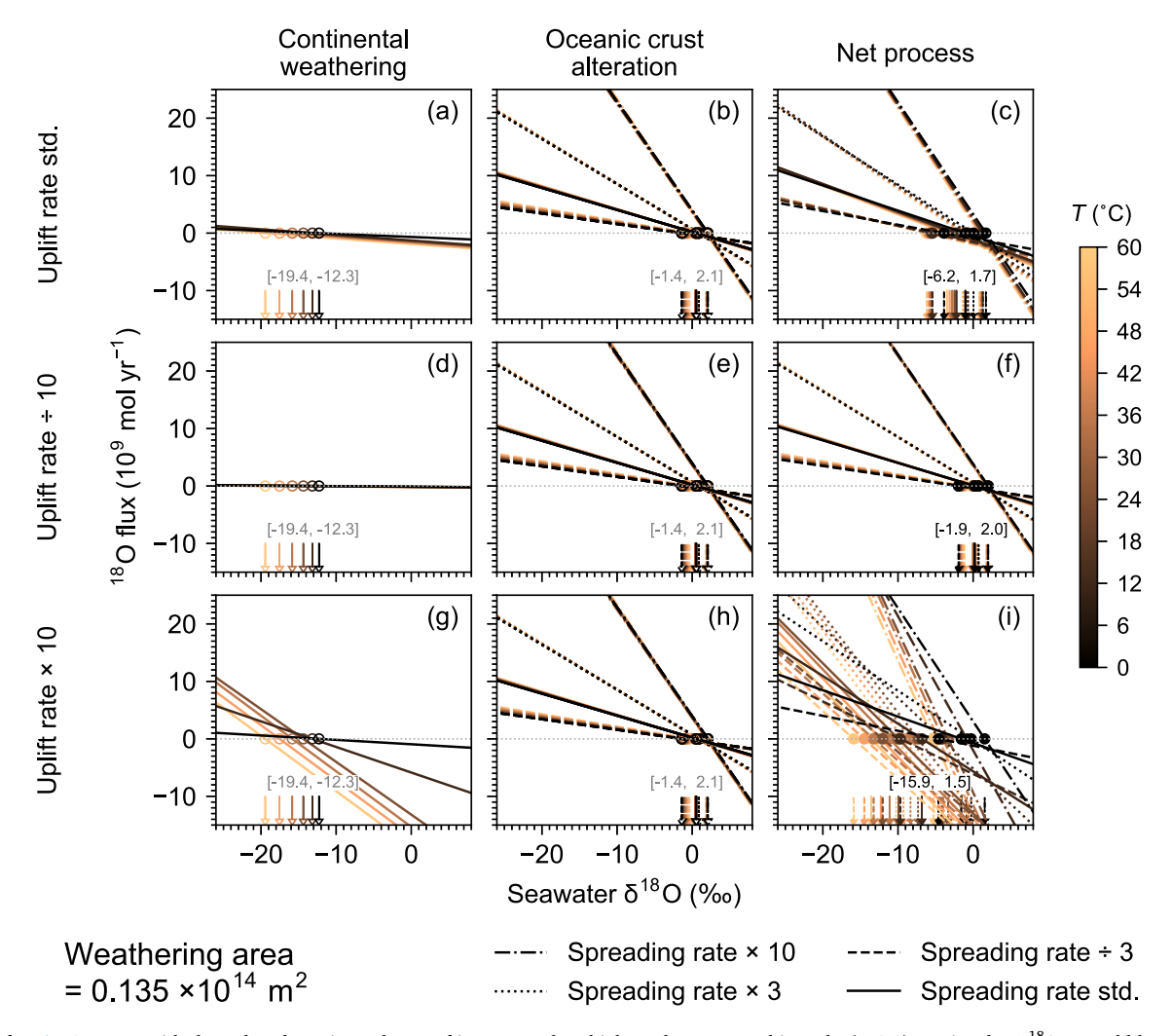


Fig. 9. As for Fig. 8 except with the reduced continental area of igneous and/or high-grade metamorphic rocks (× 0.1). Notice that $\delta^{18}O_{sw}$ would have been kept close to 0% except for the case with an enhanced uplift rate (g–i) where a negative $\delta^{18}O_{sw}$ is likely.

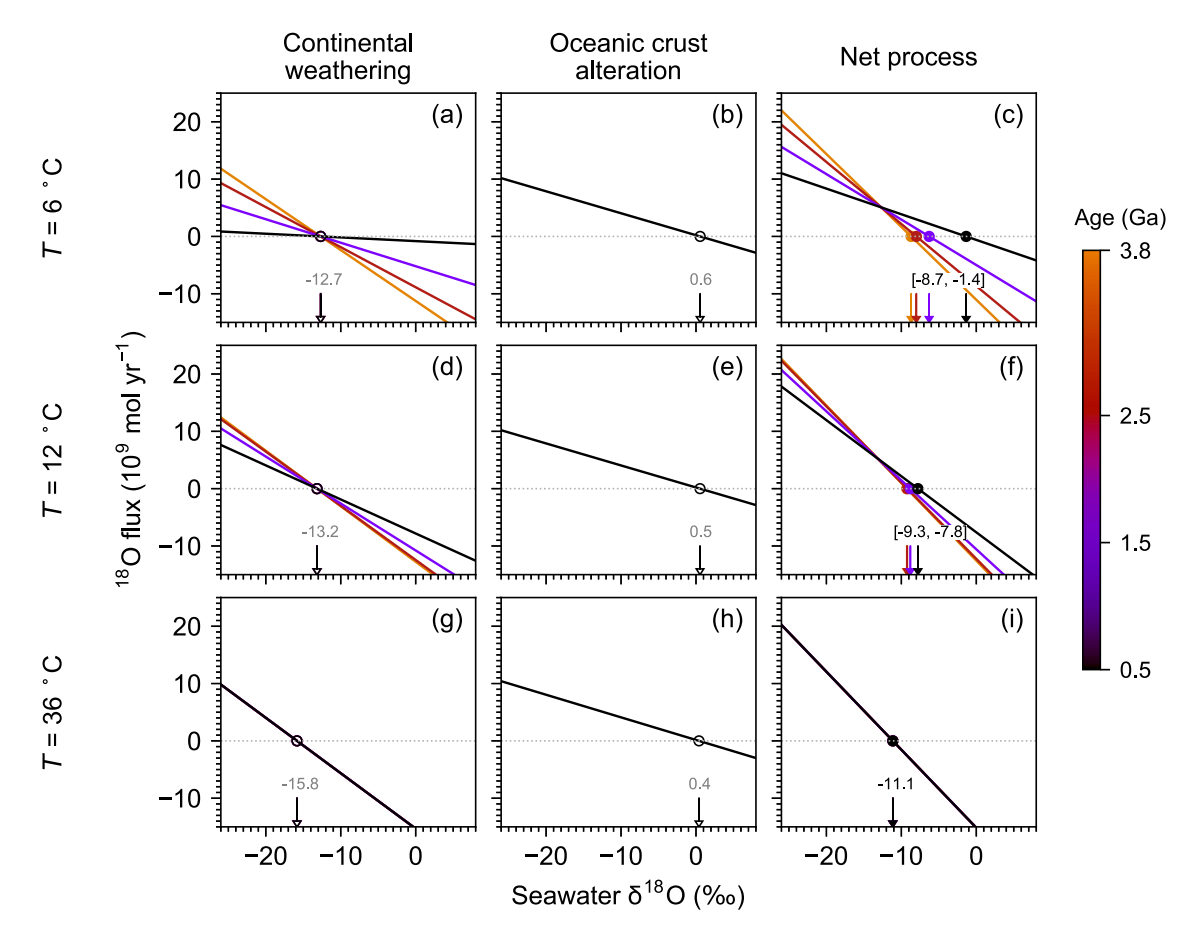
continental area and uplift rate). When isotope exchanges are limited by surface reactions at lower temperatures (the reaction-limited regime, "K" in Fig. 1), the 18 O buffering intensity changes with temperature as recognized from variable slopes in panels a, d, and g of Figs. 8 and 9. The luminosity variation (from 75% at 3.8 Ga to 95% at 0.5 Ga, of the modern value) determines if the system is in the water-buffered equilibrium regime or the reaction-limited regime for a given alteration condition (temperature and continental uplift rate), as illustrated in Fig. 10 (cf. Section 3.3.2).

When the alteration area on continents (scaled for the net weathering ^{18}O flux) became relatively large (Fig. 8), which is plausible after the major episodes of continental emergence and growth (cf. Bindeman et al., 2018), a negative value of seawater $\delta^{18}O$ which is inferred from the shale data (from -12 to -4% of $\delta^{18}O_{sw}$) can be accomplished. The exception is only the case where the uplift rate was significantly slower, or the spreading rate was significantly faster than the present-day value, e.g., by a factor of 10.

Instead, when the alteration area on continents was as small as 10% of the modern land area (likely when continents first formed, e.g., Flament et al., 2008), the negative seawater δ^{18} O can only be achieved when the uplift rate was enhanced by the same factor (10) at the same time (Fig. 9).

Overall, as long as the total volume of eroded rocks (m^3 yr $^{-1}$) equivalent to (uplift rate) \times (weathering area) stays relatively constant throughout the Earth's history, it is inevitable to have a negative

seawater $\delta^{18}O$ during the Precambrian regardless of how continents got assembled. In this case, the approach to the present-day seawater δ^{18} O (0 to -1%) can be regarded as a consequence of the shift in the dominant oxygen isotope exchange regime on the continents — from the water-buffered equilibrium regime to the reaction-limited regime enabled by a decline of atmospheric CO2 as well as expansion of sedimentary rocks blanketing the continents, and the corresponding drop of weathering contribution to the ocean ¹⁸O budget (Figs. 7-10). For instance, increasing luminosity and the corresponding decline in atmospheric CO2 level with age are enough to cause the shift in the Oisotope exchange regime and could have driven seawater δ^{18} O to evolve from -9 to -1% through the Precambrian even without any changes in the surface temperature and global runoff if the tectonic settings allow, e.g., a constant volumetric erosion rate of the continents through time (e.g., Figs. 10a-c; see above). Furthermore, when combined with a decline of temperature within a moderate climate range (e.g., between 36 and 6 °C, Fig. 10), an evolution of seawater δ^{18} O from <-10 to -1%is achieved more readily, with the corresponding decline of weathering contribution from >70% to ~10% (Figs. 10c, f and i). The above scenarios within the favorable tectonic settings (e.g., the constant volumetric erosion rate of continents) for a negative seawater $\delta^{18}O$ (e.g., Figs. 8a-c and 9g-i) provide the most parsimonious and coherent explanation of triple oxygen isotope of shales, whose trend shift during the Precambrian also indicates the shift of the dominant O-isotope exchange regime and evolution of seawater δ^{18} O (e.g., Fig. 10; cf. Section



Uplift & spreading rate = std. Weathering area = $1.35 \times 10^{14} \text{ m}^2$

Fig. 10. Effects of seawater δ^{18} O composition during the Precambrian on the 18 O fluxes from continental weathering (a, d, g) and hydrothermal alteration of oceanic crust (b, e, h), and the total 18 O flux from both processes (c, f, i). The models assume the standard values for continental uplift rate and spreading rate of oceanic crust, and the modern land area for the continental area of igneous and/or high-grade metamorphic rocks to illustrate the effects of temperature and luminosity variations. Note that solar luminosity increases 20% during the considered age span. Hypothetical steady-state seawater δ^{18} O for continental weathering and oceanic crust alteration are denoted with open arrows with their values annotated in grey in the left two columns of the diagram (a, b, d, e, g, h). Actual steady-state seawater δ^{18} O can change with luminosity or age for a given alteration condition, denoted by the correspondingly colored arrows with their values or ranges in black in the rightmost column (c, f, i).

3.3.2).

Other scenarios, especially those involving a slow uplift rate or a high spreading rate (Figs. 8 and 9), are not in accord with the triple oxygen isotope data of Archean and Proterozoic shales, unable to explain a negative seawater δ^{18} O, but could have been the case on limited geological timescales (e.g., the Hadean) or in limited geographic regions, given the huge volume of the ocean that takes a long time (e.g., $10^7 - 10^8$ yr) to reach steady state with respect to oxygen isotopes (e.g., Walker and Lohmann, 1989; Holland, 1984; Kanzaki, 2020a). Also, one may not be able to exclude scenarios where Earth's tectonics evolved to cause seawater δ^{18} O to evolve, e.g., a decline of the total O flux by weathering (= weathering area multiplied by uplift rate) or increase of the spreading rate of oceanic crust, with age (Figs. 8 and 9; cf. Korenaga et al., 2017), although they may not necessarily be coherent with the shift of O-isotope exchange regime inferred from the triple oxygen isotope data in Precambrian shales.

4.2. Consistency with other geological records in the Precambrian

A negative seawater $\delta^{18}O$ during the Precambrian is also supported by other geological sedimentary records. As an example, assuming a

constant seawater $\delta^{18}O$ value of 0% requires a lower temperature to explain shale data at an older age (Figs. 4-6), which conflicts with the high surface temperature reconstruction based on other sedimentary records such as carbonates and cherts (e.g., Knauth and Lowe, 2003; Knauth, 2005). Also, a global average surface temperature close to or less than 0 °C as the interpretation of shales with 0% seawater δ^{18} O (Figs. 4-6) is also inconsistent with the glacial records that are observed only sporadically throughout the Precambrian (e.g., Catling and Kasting, 2017). On the other hand, a negative seawater δ^{18} O is consistent with a long-standing record of carbonates and cherts, and a more recent marine iron oxides record (Galili et al., 2019). Note that the estimates of seawater δ^{18} O based on kerogen δ^{18} O are proposed to be as low as -20% at ~ 1.9 Ga but as high as +20% at ~ 2.7 Ga (Tartèse et al., 2017), and thus can be regarded as inconclusive. Previous estimates of seawater δ^{18} O based on ancient altered-rock δ^{18} O at high temperatures (e.g., Pope et al., 2012; Johnson and Wing, 2020) might contain larger uncertainties than reported (Kanzaki, 2020a) and $\delta^{18}O$ (and δD) could have varied in the Precambrian.

4.3. Insights from triple oxygen isotope systematics

Adding $^{17}{\rm O}$ to the mass balance of oxygen isotopes provides extra constraints on alteration conditions and potentially ancient tectonic styles. Firstly, observed oceanic crustal $\Delta'^{17}{\rm O}$ data can be explained only under hydrothermal alteration conditions where O-isotopic coupling between seawater and oceanic rocks is weak (Figs. 1c and d). Accordingly, the buffering of seawater $\delta^{18}{\rm O}$ by hydrothermal alteration of oceanic crust is generally weak. This conclusion is consistent with an independent argument by Kanzaki (2020a) based on typical values for kinetics of isotope exchanges and transport of water and rock (i.e., ψ and κ) calculated for hydrothermal alteration systems (see also Section 3.3.1), as well as the Earth's heat budget (Section 3.1).

Second, an explanation of observed shale ${\Delta'}^{17}O$ data requires a shift in the dominant O-isotope exchange regime for weathering as well as a negative $\delta^{18}O_{sw}$ during the Precambrian, which in turn gives us constraints on the tectonic settings of ancient Earth and their evolution (Section 4.1). Currently, however, it is difficult to examine the consistency of the alteration and tectonic conditions inferred from ${\Delta'}^{17}O$ with those from other geological observations given divergent theoretical interpretations (e.g., Veizer and Jansen, 1979; Korenaga et al., 2017). Nonetheless, this study demonstrated the utility of reactive transport models and triple oxygen isotope systematics for testing hypotheses surrounding the Precambrian climate and tectonics.

4.4. Future directions

Tripe oxygen isotope of shales indicates a shift in the weathering regime during the Precambrian (Section 3), which also means that the strength of weathering feedback on climate via drawdown of $\rm CO_2$ could have changed with time (Maher and Chamberlain, 2014; Kanzaki and Murakami, 2018a). Note, however, that the weathering regime can differ between minerals/elements/isotopes even under the same alteration condition depending on, e.g., their reaction kinetics and parentrock concentrations (e.g., Brantley et al., 2017). To make implications of weathering regime change for the Precambrian climate regulation, further examination will be required, e.g., by coupling explicit models of the global carbon cycle, climate (cf. Abbot et al., 2012; Goddéris et al., 2012; Krissansen-Totton and Catling, 2017), and oxygen isotopes.

As the current models can explain the observations of Phanerozoic and Precambrian shales and oceanic crust, our results will likely remain valid unless the alteration conditions were drastically different from those assumed in this study and/or new observations make a trend change in the overall dataset. As an example, ¹⁸O shifts of oceanic basalts via modern seafloor weathering are mostly completed within $<10^7$ years from the midocean ridge axis (Muehlenbachs, 1979), but this might not have necessarily been the case in the ancient past especially when there is no geological record available and if the modern limitation on basalt- $\delta^{18}O$ shift is caused externally (e.g., by thickening sediment cover with age; Kasting et al., 2006) rather than internally (e.g., by a decline of the isotope exchange rate with age; Kanzaki, 2020b). Such possibility can be evaluated by e.g., developing a 2D model that focuses on low-T hydrothermal fluid circulation in basalts (e.g., Farahat et al., 2017) coupled with exchanges of triple oxygen isotopes between rock and porewater, and/or by obtaining more triple oxygen isotope data from ophiolites.

5. Conclusions

 Adding ¹⁷O in rock sample data and numerical tools enables us to apply triple oxygen isotope systematics to geological records and to obtain a consistent solution of ¹⁷O/¹⁶O and ¹⁸O/¹⁶O ratios in meteoric- and/or seawaters and alteration conditions including surface temperature.

- 2) The numerical reactive transport models utilized in this study are process-based and can reproduce $\delta^{18}O$ and $\Delta'^{17}O$ data from Phanerozoic shales and oceanic crust.
- These validated models were then applied to the Precambrian rock record;
 - a. Triple oxygen isotope of shales suggests that the surface temperature could have been moderate, not drastically different from the modern and Phanerozoic values, while Precambrian seawater $\delta^{18} O$ value could have been negative and variable and likely evolved from -12 to -4 % between 3.8 and 0.5 Ga.
 - b. Negative oceanic-crustal $\Delta'^{17}O$ values also suggest that hydrothermal alteration conditions generally do not allow satisfaction of both high temperature and high water/rock ratio at the same time, and thus buffering of seawater $\delta^{18}O$ values by hydrothermal processes could have been relatively weak throughout the Earth's history.
- 4) With the inferred weak buffering, changes in surface environments including atmospheric composition could have led to a secular change in $^{18}\mathrm{O}$ flux from continental weathering and hence a seawater $\delta^{18}\mathrm{O}$ transition not dissimilar to $\delta^{18}\mathrm{O}$ records observed in sedimentary rocks; carbonates, cherts, and shales.

Declaration of Competing Interest

The authors declare that they have no known competing financial interests or personal relationships that could have appeared to influence the work reported in this paper.

Acknowledgements

We are grateful to Boswell Wing for his useful comments on the earlier version of the manuscript. We also express our gratitude to Oleg S. Pokrovsky and two anonymous reviewers for their useful comments on the current manuscript.

Appendix A. Supplementary data

Supplementary data to this article can be found online at https://doi.org/10.1016/j.chemgeo.2022.120944.

References

- Abbot, D.S., Cowan, N.B., Ciesla, F.J., 2012. Indication of insensitivity of planetary weathering behavior and habitable zone to surface land fraction. Astrophys. J. 756, 178.
- Amiotte Suchet, P., Probst, J.-L., Ludwig, W., 2003. Worldwide distribution of continental rock lithology: implications for the atmospheric/soil CO_2 uptake by continental weathering and alkalinity river transport to the oceans. Glob. Biogeochem. Cycles 17, 1038.
- Baker, E.T., Chen, Y.J., Morgan, J.P., 1996. The relationship between near-axis hydrothermal cooling and the spreading rate of mid-ocean ridges. Earth Planet. Sci. Lett. 142, 137–145.
- Berner, R.A., 2006. GEOCARBSULF: a combined model for Phanerozoic atmospheric O₂ and CO₂. Geochim. Cosmochim. Acta 70, 5653–5664.
- Berner, R.A., Lasaga, A.C., Garrels, R.M., 1983. The carbonate-silicate geochemical cycle and its effect on atmospheric carbon dioxide over the past 100 million years. Am. J. Sci. 283, 641–683.
- Bindeman, I.N., 2021. Triple oxygen isotopes in evolving continental crust, granites, and clastic sediments. Rev. Mineral. Geochem. 86, 241–290.
- Bindeman, I.N., O'Neil, J., 2022. Earth's earliest hydrosphere recorded by the oldest hydrothermally-altered oceanic crust: triple oxygen and hydrogen isotopes in the 4.3-3.8 Ga Nuvvuagittuq belt, Canada. Earth Planet. Sci. Lett. 586, 117539.
- Bindeman, I.N., Bekker, A., Zakharov, D.O., 2016. Oxygen isotope perspective on crustal evolution on early Earth: a record of Precambrian shales with emphasis on Paleoproterozoic glaciations and Great Oxygenation Event. Earth Planet. Sci. Lett. 437. 101–113.
- Bindeman, I.N., Zakharov, D.O., Palandri, J., Grever, N.D., Dauphas, N., Retallack, G.J., Hofmann, A., Lackey, J.S., Bekker, A., 2018. Rapid emergence of subaerial landmasses and onset of a modern hydrologic cycle 2.5 billion years ago. Nature 557, 545–548.
- Bindeman, I.N., Bayon, G., Palandri, J., 2019. Triple oxygen isotope investigation of finegrained sediments from major world's rivers: Insights into weathering processes and global fluxes into the hydrosphere. Earth Planet. Sci. Lett. 528, 115851.

Y. Kanzaki and I.N. Bindeman Chemical Geology 604 (2022) 120944

- Bowen, G.J., 2008. Spatial analysis of the intra-annual variation of precipitation isotope ratios and its climatological corollaries. J. Geophys. Res. 113, D05113.
- Brady, P.V., Gíslason, S.R., 1997. Seafloor weathering controls on atmospheric CO2 and global climate. Geochim. Cosmochim. Acta 61, 965-973.
- Brantley, S.L., Lebedeva, M.I., Balashov, V.N., Singha, K., Sullivan, P.L., Stinchcomb, G., 2017. Toward a conceptual model relating chemical reaction fronts to water flow paths in hills. Geomorphology 277, 100-117.
- Catling, D.C., Kasting, J.F., 2017. Atmospheric Evolution on Inhabited and Lifeless Worlds. Cambridge University Press.
- Cole, D.R., Ohmoto, H., Lasaga, A.C., 1983. Isotopic exchange in mineral-fluid systems. I. Theoretical evaluation of oxygen isotopic exchange accompanying surface reactions and diffusion. Geochim. Cosmochim. Acta 47, 1681–1693.
- Dansgaard, W., 1964. Stable isotopes in precipitation. Tellus 16, 436-468.
- DePaolo, D.J., 2011. Surface kinetic model for isotopic and trace element fractionation during precipitation of calcite from aqueous solutions. Geochim. Cosmochim. Acta 75, 1039-1056.
- Epstein, S., Buchsbaum, R., Lowenstam, A., Urey, H.C., 1953. Revised carbonate-water isotopic temperature scale. Bull. Geol. Soc. Am. 64, 1315-1326.
- Farahat, N.X., Archer, D., Abbot, D.S., 2017. Validation of the BASALT model for simulating off-axis hydrothermal circulation in oceanic crust. J. Geophys. Res. 122,
- Flament, N., Coltice, N., Rey, P.F., 2008. A case for late-Archaean continental emergence from thermal evolution models and hypsometry. Earth Planet. Sci. Lett. 275,
- Galili, N., Shemesh, A., Yam, R., Brailovsky, I., Sela-Adler, M., Schuster, E.M., Collom, C., Bekker, A., Planavsky, N., Macdonald, F.A., Préat, A., Rudmin, M., Trela, W., Sturesson, U., Heikoop, J.M., Aurell, M., Ramajo, J., Halevy, I., 2019. The geologic history of seawater oxygen isotopes from marine iron oxides. Science 365, 469–473.
- Goddéris, Y., Donnadieu, Y., Lefebvre, V., Le Hir, G., Nardin, E., 2012. Tectonic control of continental weathering, atmospheric CO2, and climate over Phanerozoic times. Compt. Rendus Geosci. 344, 652–662.
- Gough, D.O., 1981. Solar interior structure and luminosity variations. Sol. Phys. 74,
- Gregory, R.T., 1991. Oxygen isotope history of seawater revisited: Timescales for boundary event changes in the oxygen isotope composition of seawater. In: Taylor Jr., H.P., O'Neil, J.R., Kaplan, I.R. (Eds.), Stable Isotope Geochemistry: A Tribute to Samuel Epstein. The Geochemical Society, pp. 65-76.
- Gregory, R.T., Taylor Jr., H.P., 1981. An oxygen isotope profile in a section of cretaceous oceanic crust, Samail ophiolite, Oman: evidence for δ^{18} O buffering of the oceans by deep (>5km) seawater-hydrothermal circulation at mid-ocean-ridges. J. Geophys. Res. 86, 2737-2755.
- Herwartz, D., 2021. Triple oxygen isotope variations in Earth's crust. Rev. Mineral. Geochem. 86, 291–322.
- Herwartz, D., Pack, A., Krylov, D., Xiao, Y., Muehlenbachs, K., Sengupta, S., Di Rocco, T., 2015. Revealing the climate of snowball Earth from Δ^{17} O systematics of hydrothermal rocks. Proc. Natl. Acad. Sci. U. S. A. 112, 5337–5341.
- Holland, H.D., 1984, The Chemical Evolution of the Atmosphere and Oceans, Princeton University Press.
- Holmden, C., Muehlenbachs, K., 1993. The ¹⁸O/¹⁶O ratio of 2-billion-year-old seawater inferred from ancient oceanic crust. Science 259, 1733-1736.
- Husson, J.M., Peters, S.E., 2017. Atmospheric oxygenation driven by unsteady growth of the continental sedimentary reservoir. Earth Planet. Sci. Lett. 460, 68-75.
- Jaffrés, J.B.D., Shields, G.A., Wallmann, K., 2007. The oxygen isotope evolution of seawater: a critical review of a long-standing controversy and an improved geological water cycle model for the past 3.4 billion years. Earth-Sci. Rev. 83, 83-122
- Johnson, B.W., Wing, B.A., 2020. Limited Archaean continental emergence reflected in an early Archaean ¹⁸O-enriched ocean. Nat. Geosci. 13, 243–248.
- Kanzaki, Y., 2020a. Interpretation of oxygen isotopes in Phanerozoic ophiolites and sedimentary rocks. Geochem. Geophys. Geosyst. 21 e2020GC009000.
- Kanzaki, Y., 2020b. Quantifying the buffering of oceanic oxygen isotopes at ancient midocean ridges. Solid Earth 11, 1475-1488.
- Kanzaki, Y., Murakami, T., 2018a. Effects of atmospheric composition on apparent activation energy of silicate weathering: I. Model formulation. Geochim. Cosmochim. Acta 233, 159-186.
- Kanzaki, Y., Murakami, T., 2018b. Effects of atmospheric composition on apparent activation energy of silicate weathering: II. Implications for evolution of atmospheric ${\rm CO_2}$ in the Precambrian. Geochim. Cosmochim. Acta 240, 314–330.
- Kasting, J.F., Howard, M.T., Wallmann, K., Veizer, J., Shields, G., Jaffrés, J., 2006. Paleoclimates, ocean depth, and the oxygen isotopic composition of seawater. Earth Planet. Sci. Lett. 252, 82-93.
- Knauth, L.P., 2005. Temperature and salinity history of the Precambrian ocean: implications for the course of microbial evolution. Palaeogeogr. Palaeoclimatol. Palaeoecol, 219, 53-69.
- Knauth, L.P., Lowe, D.R., 2003. High Archean climatic temperature inferred from oxygen isotope geochemistry of cherts in the 3.5 Ga Swaziland Supergroup, South Africa. Geol. Soc. Am. Bull. 115, 566-580.
- Korenaga, J., Planavsky, N.J., Evans, D.A.D., 2017. Archean geodynamics and the thermal evolution of Earth. Phil. Trans. R. Soc. A 375, 20150393.
- Krissansen-Totton, J., Catling, D.C., 2017. Constraining climate sensitivity and continental versus seafloor weathering using an inverse geological carbon cycle model. Nat. Commun. 8, 15423.
- Le Hir, G., Donnadieu, Y., Goddéris, Y., Pierrehumbert, R.T., Halverson, G.P., Macouin, M., Nédélec, A., Ramstein, G., 2009. The snowball Earth aftermath: exploring the limits of continental weathering processes. Earth Planet. Sci. Lett. 277, 453-463.

- Liljestrand, F.L., Knoll, A.H., Tosca, N.J., Cohen, P.A., Macdonald, F.A., Peng, Y., Johnson, D.T., 2020. The triple oxygen isotope composition of Precambrian chert.
- Earth Planet. Sci. Lett. 537, 116167. Luz, B., Barkan, E., 2010. Variations of ¹⁷O/¹⁶O and ¹⁸O/¹⁶O in meteoric waters. Geochim. Cosmochim. Acta 72, 6276-6286.
- Maher, K., Chamberlain, C.P., 2014. Hydrologic regulation of chemical weathering and the geologic carbon cycle. Science 343, 1502–1504.
 Miller, M.F., Pack, A., 2021. Why measure ¹⁷O? Historical perspective, triple-isotope
- systematics and selected applications. Rev. Mineral. Geochem. 86, 1-34.
- Miller, M.F., Pack, A., Bindeman, I.N., Greenwood, R.C., 2020. Standardizing the reporting of Δ¹⁷O data from high precision oxygen triple-isotope ratio measurements of silicate rocks and minerals. Chem. Geol. 532, 119332.
- Muehlenbachs, K., 1979. The alteration and aging of the basaltic layer of the seafloor: oxygen isotope evidence from DSDP/IPOD Legs 51, 52, and 53. Int. Repts. DSDP 51,
- Muehlenbachs, K., 1998. The oxygen isotopic composition of the oceans, sediments and the seafloor. Chem. Geol. 145, 263-273.
- Muehlenbachs, K., Clayton, R.N., 1976. Oxygen isotope composition of the oceanic crust and its bearing on seawater. J. Geophys. Res. 81, 4365-4369.
- Pack, A., Herwartz, D., 2014. The triple oxygen isotope composition of the Earth mantle and understanding Δ^{17} O variations in terrestrial rocks and minerals. Earth Planet. Sci. Lett. 390, 138-145.
- Perry Jr., E.C., Ahmad, S.N., Swulius, T.M., 1978. The oxygen isotope composition of 3,800 my old metamorphosed chert and iron formation from Isukasia, West Greenland. J. Geol. 86, 223-239.
- Pope, E.C., Bird, D.K., Rosing, M.T., 2012. Isotope composition and volume of Earth's early oceans. Proc. Natl. Acad. Sci. U. S. A. 109, 4371–4376.
- Royer, D.L., Donnadieu, Y., Park, J., Kowalczyk, J., Goddéris, Y., 2014. Error analysis of CO₂ and O₂ estimates from the long-term geochemical model GEOCARBSULF. Am. J. Sci. 314, 1259-1283.
- Ryb, U., Eiler, J.M., 2018. Oxygen isotope composition of the Phanerozoic ocean and a possible solution to the dolomite problem. Proc. Natl. Acad. Sci. U. S. A. 115, 6602-6607.
- Schauble, E.A., Young, E.D., 2021. Mass dependence of equilibrium oxygen isotope fractionation in carbonate, nitrate, oxide, perchlorate, phosphate, silicate, and sulfate minerals, Rev. Mineral, Geochem, 86, 137-178.
- Sengupta, S., Peters, S.T.M., Reitner, J., Duda, J.-P., Pack, A., 2020. Triple oxygen isotopes of cherts through time. Chem. Geol. 554, 119789.
- Sharp, Z.D., Wostbrock, J.A.G., 2021. Standardization for the triple oxygen isotope system; waters, silicates, carbonates, air, and sulfates, Rev. Mineral, Geochem, 86, 179-196.
- Sharp, Z.D., Gibbon, J.A., Maltsev, O., Atudorei, V., Pack, A., Sengupta, S., Shock, E.L., Knauth, L.P., 2016. A calibration of the triple oxygen isotope fractionation in the SiO₂-H₂O system and applications to natural samples. Geochim. Cosmochim. Acta 186, 105-119.
- Sharp, Z.D., Wostbrock, J.A.G., Pack, A., 2018. Mass-dependent triple oxygen isotope variations in terrestrial materials. Geochem. Persp. Lett. 7, 27–32.
- Shields, G., Veizer, J., 2002. Precambrian marine carbonate isotope database: Version 1.1. Geochem. Geophys. Geosyst. 3 https://doi.org/10.1029/2001GC000266.
- Tartèse, R., Chaussidon, M., Gurenko, A., Delarue, F., Robert, F., 2017. Warm Archean oceans reconstructed from oxygen isotope composition of early-life remnants. Geochem. Persp. Lett. 3, 55-65.
- Taylor Jr., H.P., 1968. The oxygen isotope geochemistry of igneous rocks. Contrib. Mineral. Petrol. 19, 1-71.
- Urey, H.C., Lowenstam, A., Epstein, S., McKinney, C.R., 1951, Measurement of paleotemperatures and temperatures of the Upper Cretaceous of England, Denmark, and the southeastern United States. Bull. Geol. Soc. Am. 62, 399–416. Veizer, J., Hoefs, J., 1976. The nature of O^{18}/O^{16} and C^{13}/C^{12} secular trends in
- sedimentary carbonate rocks. Geochim. Cosmochim. Acta 40, 1387-1395.
- Veizer, J., Jansen, S.L., 1979. Basement and sedimentary recycling and continental evolution. J. Geol. 87, 341-370.
- Veizer, J., Prokoph, A., 2015. Temperatures and oxygen isotopic composition of Phanerozoic oceans. Earth-Sci. Rev. 146, 92-104.
- Veizer, J., Ala, D., Azmy, K., Bruckschen, P., Buhl, D., Bruhn, F., Carden, G.A., Diener, A., Ebneth, S., Godderis, Y., Jasper, T., Korte, C., Pawellek, F., Podlaha, O.G., Strauss, H., 1999. 87 Sr/ 86 Sr, δ^{13} C and δ^{18} O evolution of Phanerozoic seawater. Chem. Geol. 161, 59-88.
- Vérard, C., Veizer, J., 2019. On plate tectonics and ocean temperatures. Geology 47, 881-885.
- von Paris, P., Rauer, H., Grenfell, J.L., Patzer, B., Hedelt, P., Stracke, B., Trautmann, T., Schreier, F., 2008. Warming the early Earth—CO₂ reconsidered. Planet. Space Sci. 56, 1244-1259.
- Walker, J.C.G., Lohmann, K.G., 1989. Why the oxygen isotopic composition of sea water changes with time. Geophys. Res. Lett. 16, 323-326.
- Wallmann, K., 2001. The geological water cycle and the evolution of marine δ^{18} O values. Geochim. Cosmochim. Acta 65, 2469-2485.
- Wostbrock, J.A.G., Sharp, Z.D., 2021. Triple oxygen isotopes in silica-water and carbonate-water systems. Rev. Mineral. Geochem. 86, 367-400.

- Zakharov, D.O., Bindeman, I.N., 2019. Triple oxygen and hydrogen isotopic study of hydrothermally altered rocks from the 2.43–2.41 Ga Vetreny belt, Russia: an insight into the early Paleoproterozoic seawater. Geochim. Cosmochim. Acta 248, 185–209.
- into the early Paleoproterozoic seawater. Geochim. Cosmochim. Acta 248, 185-209. Zakharov, D.O., Bindeman, I.N., Tanaka, R., Friòleifsson, G.Ó., Reed, M.H., Hampton, R. L., 2019. Triple oxygen isotope systematics as a tracer of fluids in the crust: a study from modern geothermal systems of Iceland. Chem. Geol. 530, 119312.
- Zakharov, D.O., Lundstrom, C.C., Laurent, O., Reed, M.H., Bindeman, I.N., 2021. Influence of high marine Ca/SO_4 ratio on alteration of submarine basalts at 2.41 Ga documented by triple O and Sr isotopes of epidote. Precambrian Res. 358, 106164.